LBL-10540
CERRO-PRIETO-11
UC-66b

# MEXICAN-AMERICAN COOPERATIVE PROGRAM AT THE CERRO PRIETO GEOTHERMAL FIELD

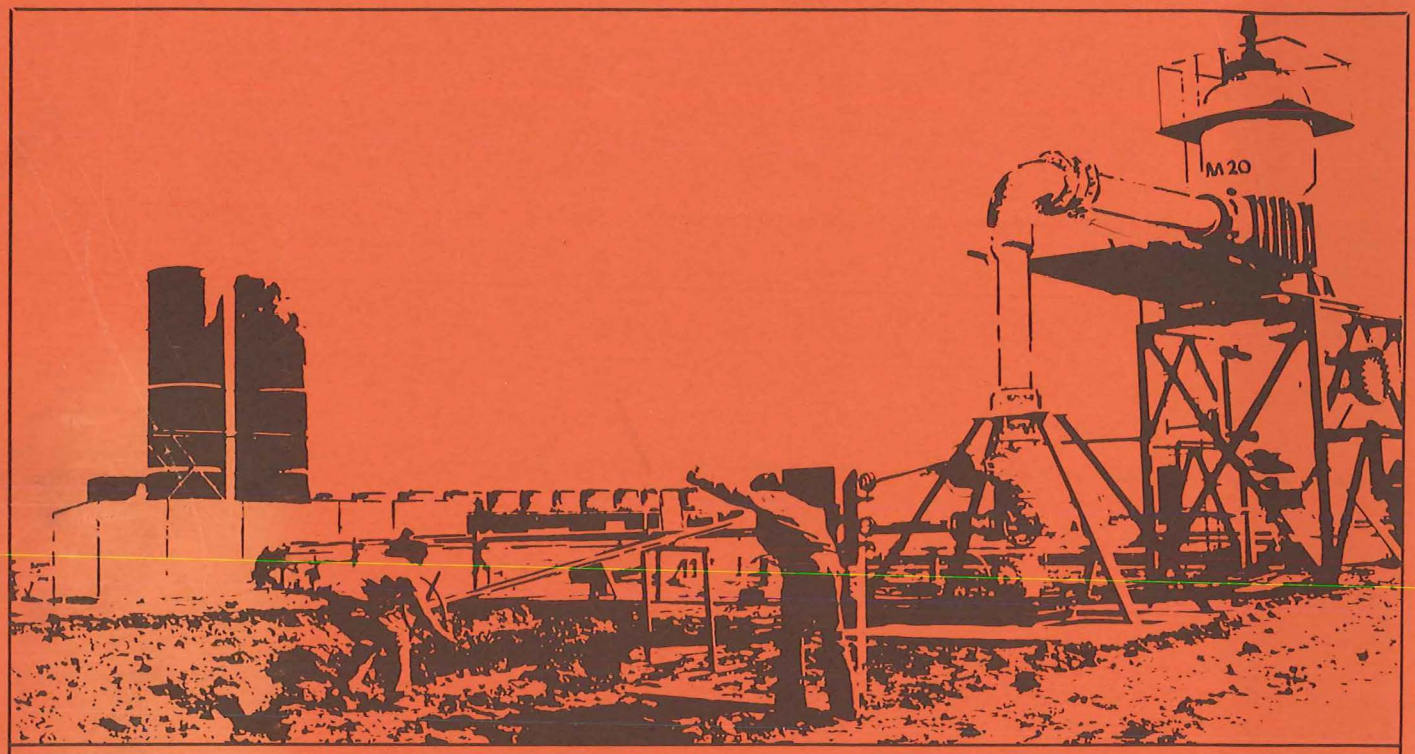


# SUBSURFACE GEOLOGICAL AND GEOPHYSICAL STUDY OF THE CERRO PRIETO GEOTHERMAL FIELD BAJA CALIFORNIA, MEXICO

D. J. Lyons and P. C. van de Kamp

GeoResources Associates
Napa, California

January 1980

A Joint Project of

COMISION FEDERAL DE ELECTRICIDAD
Mèxico

DEPARTMENT OF ENERGY
Division of Geothermal Energy
United States of America

Coordinated by

Coordinadora Ejecutiva
de Cerro Prieto
Apdo. Postal No. 3-636
Mexicali, Bja. Cfa., México
and P. O. Box 248
Calexico, Ca. 92231

Lawrence Berkeley Laboratory
Earth Sciences Division
University of California
Berkeley, California 94720

Operating for the U.S. Department of
Energy under Contract W-7405-ENG-48

Printed in the United States of America
Available from
National Technical Information Service
U.S. Department of Commerce
5285 Port Royal Road
Springfield, VA 22161
Price Code: A06

LBL-10540
CP-11

# SUBSURFACE GEOLOGICAL AND GEOPHYSICAL STUDY OF THE CERRO PRIETO GEOTHERMAL FIELD, BAJA CALIFORNIA, MEXICO

D. J. Lyons and P. C. van de Kamp

GeoResources Associates

Napa, California

January 1980

Prepared for

Earth Sciences Division
Lawrence Berkeley Laboratory
University of California
Berkeley, California 94720

CONTENTS

TECHNICAL INFORMATION DEPARTMENT
LAWRENCE BERKELEY LABORATORY
UNIVERSITY OF CALIFORNIA
Berkeley, California 94720

LBL-10540
CP-11
UC-66b

November 10, 1980

To: Recipients of LBL-10540

From: Technical Information Department

ERRATA FOR REPORT LBL-10540

"Subsurface Geological and Geophysical Study of the Cerro Prieto Geothermal Field, Baja California, Mexico" by D.J. Lyons and P.C. van de Kamp

THE CAPTIONS OF THE FIGURES ON THE FOLLOWING PAGES SHOULD BE CHANGED TO:

Page 42:

Figure 15. Basin fill facies and basin margin configuration southwest of the Cerro Prieto field; northeast-southwest cross-section extends from well M-6 to the Sierra de Cucapa following seismic line D-D' (connects with geologic cross-section III-III' of Fig. 6 which is not at the same scale). Scale is approximately 1:48,000 or 1 inch equals 1200 meters or 4000 feet.

Page 73:

Figure 28. Photomicrograph of sandstone core sample from well M-20, at 915.3 m depth, plane polarized light. The dotted areas in this view are pores mostly resulting from removal of carbonate cement and feldspar. Elsewhere in this section, the cement is present. Measured porosity is 23.7% in this rock. View is 0.9 mm across.

Page 74:

Figure 29. Sandstone, well M-96 at 1979 m depth. This is a fine-grained, moderate to well-sorted rock, with secondary porosity shown in a dot pattern. The grain in the center is a partly leached feldspar. View is 0.4 mm across.

Page 75:

Figure 30. Photomicrograph of sandstone at 915.3 m depth in well M-20 showing porosity in dot pattern. On the bottom of the view is an area cemented by carbonate. The packing arrangement of detrital grains is similar in both cemented and cement-free areas. View is 0.8 mm across.

Page 76:

Figure 31. Sandstone in well M-96 composed of angular to well-rounded grains. Dotted areas are pores. In the lower left center of the view is a feldspar grain with four holes resulting from partial leaching of the grain. This sample is from 1981 m depth. View is 0.8 mm across.

ABSTRACT

The Cerro Prieto geothermal field is located near the southwestern margin of the Colorado River delta in the Mexicali Valley, which is part of the seismically active Salton Trough/Gulf of California rift basin system. The Cenozoic stratigraphic record in the Imperial Valley to the north and the geologic history of the Colorado River suggest that the southwesterly progradation of the Colorado delta across the marine rift basin began in middle Pliocene and was essentially complete by late Pliocene.

The subsurface stratigraphy at Cerro Prieto is characterized by complex vertical and lateral variations in lithofacies, which is typical of deltaic deposits. The geothermal production zone is not a uniform reservoir layer overlain by a laterally continuous top-seal of low-permeability strata.

The deeper part of the stratigraphic section in the main producing area including the productive intervals represents lower delta plain deposits of the ancestral Colorado delta. A thick predominantly sand sequence just west of the main producing area is interpreted as a deltaic coastal complex in a tide- or tide/wave-dominated delta. The area between the coastal-deltaic deposits and the basin margin alluvial fans to the west was probably an area of at least intermittent marine deposition until the middle Pleistocene.

In addition to the northeast-southwest and northwest-southeast fault trends, which have been emphasized in earlier fault interpretations of the Cerro Prieto area, north-south and north northeast-south southwest trends are also prominent. Older faults, reactivated older faults, and younger faults are present in the field. There does not seem to be any convincing geophysical evidence for a basement horst underlying the field, as suggested by various workers in the past. Instead, there is apparently a general deepening of the

basement in a southeasterly direction across the field.

The top of the hydrothermal alteration zone has a dome-like configuration which cuts across the sedimentary strata. Shales in the altered zone exhibit high densities and high resistivities on the well logs. Except for the relatively cool, shallow production on the northwest flank of the Cerro Prieto field, the geothermal production intervals generally straddle or underlie the top of the high-resistivity, high-density shales.

Sandstones in the hydrothermal alteration zone commonly have fair to good porosities (15% to 35% or higher), which resulted from the removal by solution of unstable grains and carbonate cement. Open fractures appear to be unusual in the altered zone based on core descriptions. While fractures may be an important contributor to reservoir permeability locally, secondary matrix porosity and permeability are considered to be more important volumetrically in the Cerro Prieto reservoirs.

It appears that the older faulting of the basin fill, the densification of sediments by hydrothermal alteration, and the onset of Quaternary volcanism northwest of the Cerro Prieto field were roughly synchronous. The date of the oldest known eruption at the Cerro Prieto volcano (approximately $10^5$ yr B.P.) may be a minimum age for this major thermal-tectonic "event." Episodic thermal and tectonic activity occurred from this event to the present. The secondary solution porosity in the altered sandstones developed during this period. There may have been localized cooling in some areas since the "main" thermal-tectonic event.

Surface geophysical detection of geothermal anomalies in the Cerro Prieto region may be difficult from resistivity, magnetic, or gravity data. The occurrence of a reflection-poor zone coincident with the hydrothermal alteration zone at East Mesa and at Cerro Prieto suggests that the seismic reflection method may be a good approach, but other types of geophysical

data are necessary to eliminate alternate sources of reflection-poor zones on seismic profiles.

## 1. INTRODUCTION

The subsurface investigation of the Cerro Prieto field and surrounding area described below was undertaken to provide information on the stratigraphy, structure, hydrothermal alteration, and reservoir properties for use in designing reservoir simulation models and for planning development of the field. Another objective was to gain insight into the depositional, tectonic, and thermal history of the Cerro Prieto area. Since 1975 numerous geological and geophysical studies of the Cerro Prieto geothermal field have been published or presented at technical meetings by investigators from the Comisión Federal de Electricidad de México (CFE), Lawrence Berkeley Laboratory (LBL) of the University of California, the U. S. Geological Survey, the University of California at Riverside, and several other organizations. Specific studies used are referred to throughout this report.

The following types of data were used in this study: (1) well sample descriptions and analyses (x-ray diffraction, petrography, and porosity-permeability determinations); (2) well logs (spontaneous potential, resistivity, gamma-ray, density, sonic and caliper); (3) geophysical surveys (resistivity, gravity, magnetics, refraction seismic, reflection seismic, and seismicity); (4) physiography (modern depositional patterns and surface manifestations of faults); and (5) regional geology.

The detailed interpretation of the subsurface geology presented in this report should be useful for field development. A simplified version will be necessary for reservoir simulation modeling. The approach taken in the study

and the concepts developed herein may be applicable to geothermal exploration and field development in other sedimentary basins.

## 2. STRATIGRAPHIC FRAMEWORK

### General Depositional Setting

The Cerro Prieto geothermal field is located near the southwestern margin of the Colorado River delta in the Mexicali Valley, which is part of the seismically active Salton Trough/Gulf of California rift basin system (Figure 1). Paleontologic data indicate a Miocene age for the oldest sediments in the Imperial Valley to the north and in the Gulf of California to the south (Elders and Biehler, 1975; Wagoner, 1977). Although the oldest sediments in the field have not been dated, the regional data imply that rift basin deposition began in the Cerro Prieto area during the Miocene as well; the deeper sediments are older. The Cenozoic stratigraphy in the Imperial Valley (Wagoner, 1977) and the geologic history of the Colorado River (Hunt, 1969) suggest that the progradation of the Colorado delta across the marine rift basin began in the middle Pliocene. By late Pliocene, the southwesterly advance of the delta was essentially complete, which resulted in the conversion of the Salton basin to a nonmarine depocenter and delta plain deposition in the Cerro Prieto area.

Some workers have suggested that the deltaic sediments of the main producing area intertongue with alluvial fan sediments derived from the Cucapa Range to the west (e.g. Puente C. and de la Peña L., 1979). A different interpretation of the stratigraphic relationships in the Cerro Prieto area will be developed below.

### Lithofacies Analysis

One of the main controls on the geometry, volume and recharge/discharge of the geothermal reservoir is the distribution of porosity and permeability

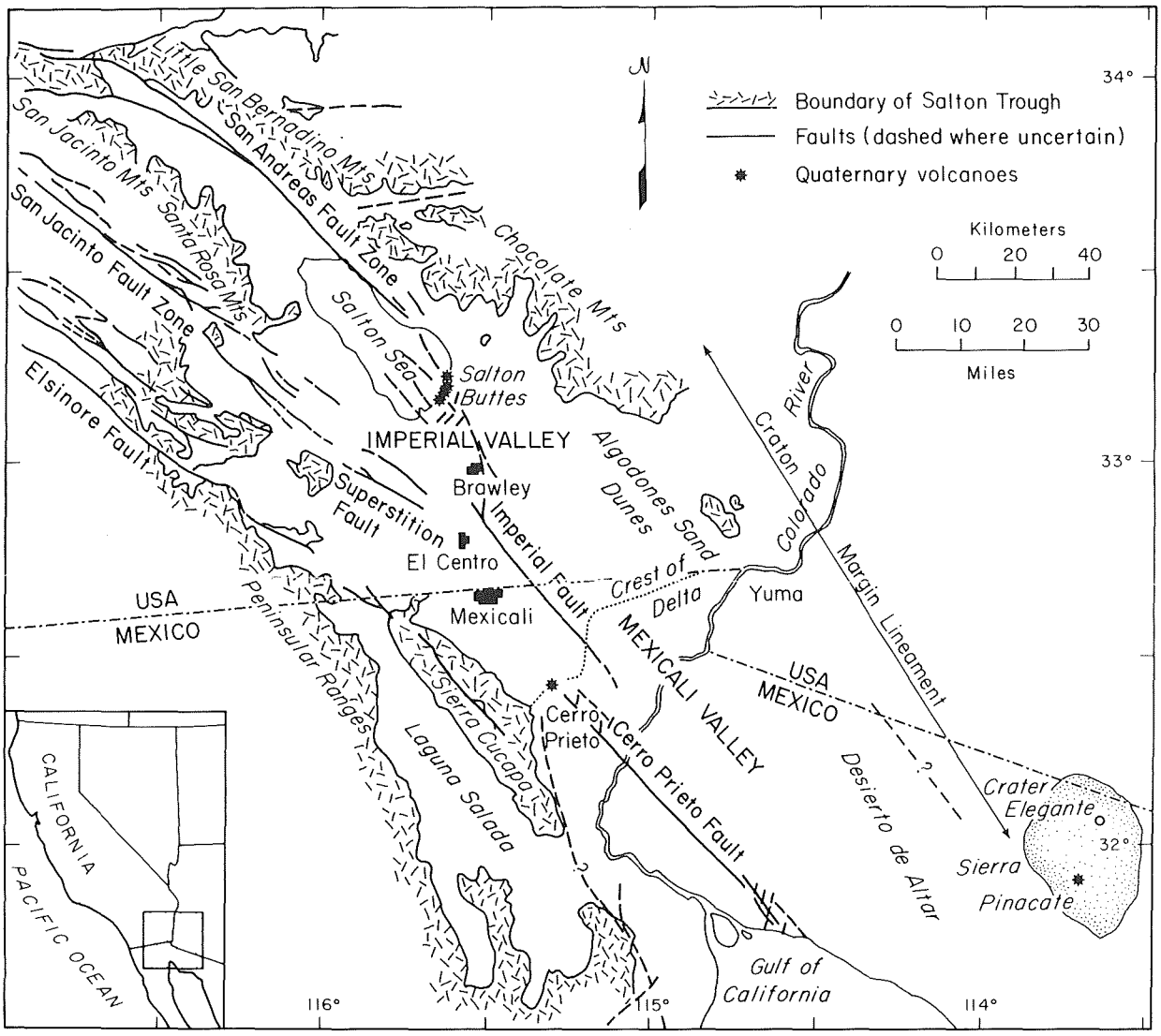


Figure 1. Location of the Cerro Prieto geothermal field (Elders, 1979, Fig. 1).

in the subsurface. Permeability results from matrix porosity and/or fractures. Matrix porosity and permeability depend on lithology (depositional texture) and on post-depositional modifications by diagenesis and metamorphism. The main purpose of this section is to illustrate the three-dimensional variations in subsurface lithology at Cerro Prieto which represents one aspect of the permeability distribution.

Deltaic strata are characterized by a complex vertical and lateral arrangement of lithologic units for the following reasons. First, deltas comprise a diversity of depositional environments that may include some or all of the following, depending on the interaction of river discharge, waves, and tides: distributary channel, levee, delta plain/swamp, bay, tidal flat including tidal channels, distributary-mouth bar, lagoon, coastal barrier, fringe (shoreface), and tidal bars and shoals. Second, diversion and abandonment of distributary channels and relative sea level changes result in repeated shifting of depositional environments.

Four cross sections were constructed for the Cerro Prieto geothermal field to illustrate the stratigraphic complexities of the subsurface, including both the older producing area and the new area currently being developed to the east (refer to the index map in Figure 2). Sections I-I′ and II-II′ are nearly transverse and sections III-III′ and IV-IV′ are nearly longitudinal with respect to a southwest-to-westerly progradation of the Colorado delta. Sections I-I′ and III-III′ closely follow seismic reflection profiles for most of their lengths.

The first step in constructing subsurface stratigraphic cross sections is to determine the stratigraphic or lithologic sequences penetrated by the wells along the line of section. Subsurface sample descriptions and wire-line (geophysical) well logs are used for this purpose.

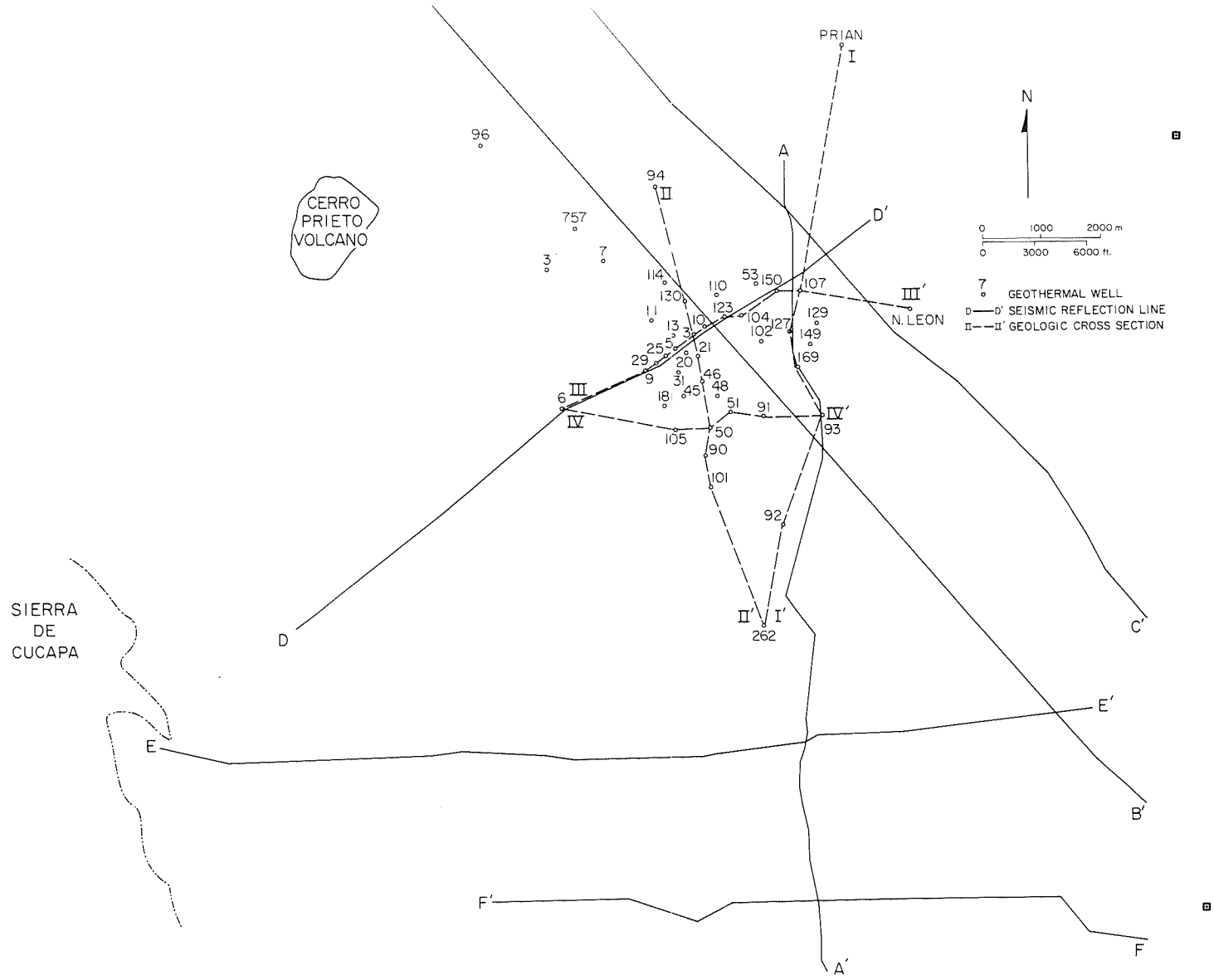


XBL 801-6752

Figure 2. Index map showing well locations, stratigraphic cross sections, and reflection seismic profiles.

In the correlation sections of Elders et al. (1978), the subsurface stratigraphy in the Cerro Prieto field is represented by sandstone percentage logs derived from cuttings descriptions. Such lithologic logs may be very misleading due to problems inherent in drilling. First, where unconsolidated sands are interbedded with fine-grained sediments, sand recovery is commonly very poor resulting in the section being logged as dominantly fine-grained sediments. Thus, sand percentage is often underestimated in the shallow part of the section. Second, caving of the borehole wall results in continued recovery of the up-hole lithology while a new lithologic unit is being drilled, which causes some lithologic units to be overestimated. Finally, a less serious problem, there is a lag between the actual depths of lithologic transitions and the depths shown on the lithologic log due to the time required for the recovery of the cuttings. For these reasons, lithologic logs derived only from cuttings descriptions are not satisfactory for illustrating the subsurface stratigraphic framework.

In subsurface studies, reduced wire-line log curves are often used to represent the lithologic sequence on stratigraphic cross sections. This approach was not taken in this study for two reasons. First, to illustrate the stratigraphic relationships from the surface down to the total depths of the Cerro Prieto wells without vertical exaggeration, the degree of log reduction necessary for a convenient cross section size would have resulted in a loss of stratigraphic information. Second, interpreting lithology from a single log curve, such as spontaneous potential (SP) or gamma-ray, is often very difficult in the Cerro Prieto wells because of pore-water salinity variations in the shallower section and complex hydrothermal alterations in the deeper section. We have observed that many

sands in the unaltered section exhibit an anomalous SP response (suppressed or reversed) accompanied by high resistivity and "normal" density, which indicates low-salinity pore waters. Based on the SP log alone, such intervals could be misinterpreted as shales or silts. Conversely, in the hydrothermally altered section, the gamma-ray curve commonly loses its character while the SP curve normally discriminates between the hot brine sandstones and the altered shales. Thus, based on the gamma-ray curve alone, lithologic discrimination in the unaltered zone is generally good, but in the altered zone is often difficult. The resistivity and density curves are also frequently helpful in determining the lithologic sequence, but the criteria are variable.

Detailed lithologic sequences were interpreted for Cerro Prieto wells by utilizing the SP, gamma-ray, resistivity, and density curves and by calibrating the log response patterns with lithologic data (i.e., cuttings and core descriptions). To illustrate the vertical and lateral stratigraphic variations in the subsurface at Cerro Prieto, these detailed lithologic sequences had to be simplified because of display scale limitations.

The approach taken in this study was to construct lithofacies columns for the wells on the cross sections based on the lithologic sequences interpreted from the well logs (wire-line, not lithologic) and the lithologic descriptions (cuttings and cores). After a preliminary analysis of the lithologic sequences penetrated by several wells in the field, five lithofacies classes were defined ranging from predominantly sand (I) to predominantly silt/shale (V). Lithofacies classes II, III, and IV were differentiated primarily by the thickness distribution of sand depositional units. Five lithofacies classes do not represent particular depositional

environments. Examples of SP curves for the lithofacies classes based on SP curves are given in Figure 3. As mentioned above, it was often necessary to use other log curves to interpret the lithologic sequence. Consequently, in some parts of the section, the lithofacies classes were interpreted from gamma-ray, resistivity, and/or density log curves using the same curve shape patterns for classification.

Lithofacies I is characterized predominantly by sand with very thick sand units (commonly greater than 150 ft or 46 m) separated by thin shale beds (less than 10 ft or 3 m). This lithofacies suggests stacked channels or possibly eolian deposits.

Lithofacies II consists dominantly of sand with sand unit thicknesses up to 50 ft (15 m) or more and shale unit thicknesses up to 20-30 ft (6-9 m). On the logs, the thicker sand units frequently appear as cylindrical or "blocky" curves with abrupt lower boundaries that suggest channels. The thinner sands may represent either channel overbank sands on the delta plain or delta-front sands; the log shape and position in the stratigraphic sequence may distinguish between these two depositional environments.

Lithofacies III is characterized by roughly equal sand and shale percentages, although sand may be dominant in some cases. The thicker sands are 20-30 ft (6-9 m) thick and have transitional bases. These features and the association with thinner sands, silts, and shales suggest a delta-front environment. However, some of this lithofacies may represent distributary overbank deposition on the delta plain.

Lithofacies IV also consists of nearly equal sand and shale percentages, but the sands are thinner than 10 ft (3 m). This lithofacies may represent

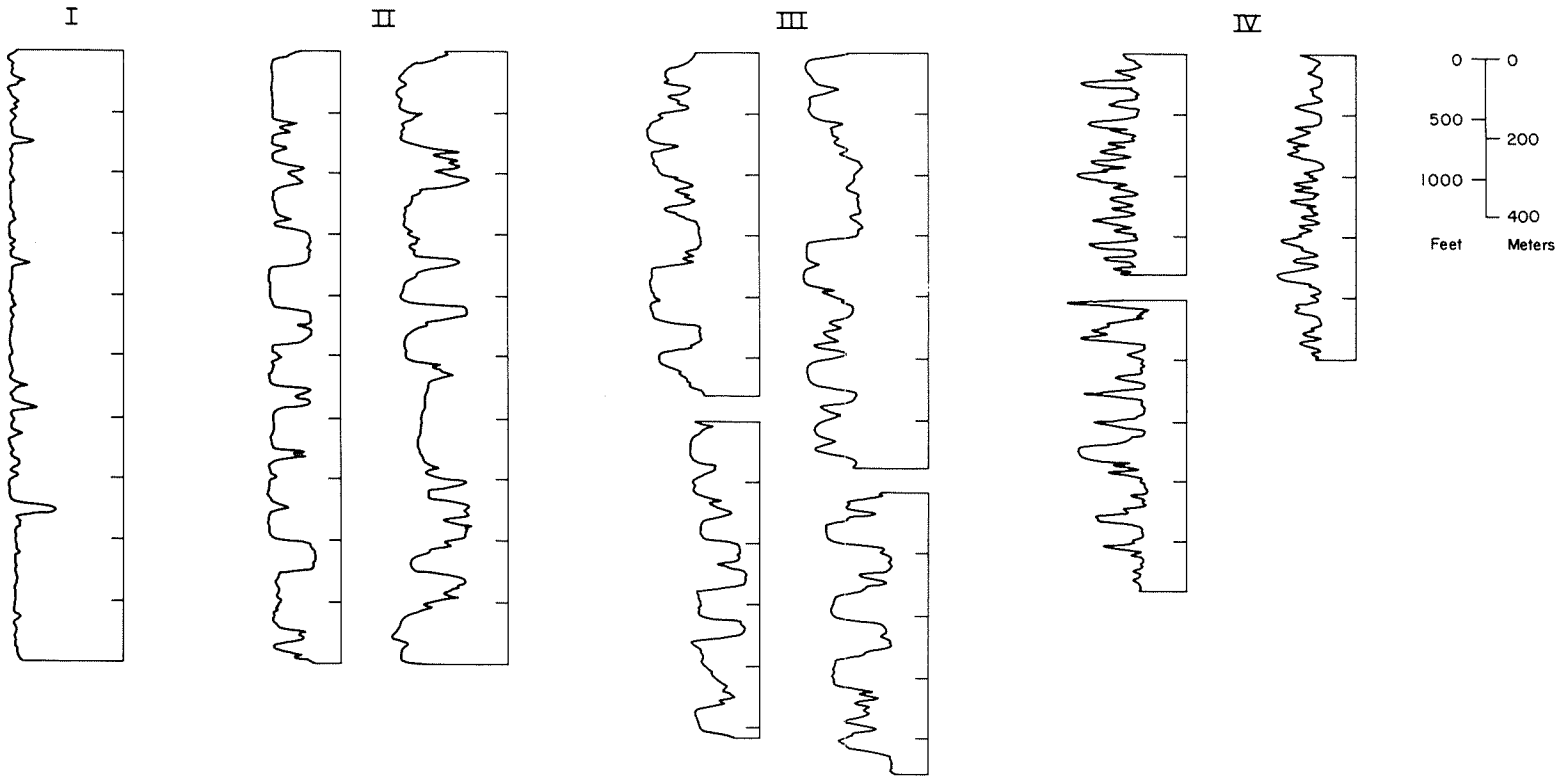


Figure 3. Examples of the lithofacies classes based on the spontaneous potential (SP) curve.

either "distal" overbank deposition on the delta plain or lower energy delta-front deposition ("outer fringe").

Lithofacies V consists dominantly of silt and shale and may represent a variety of depositional environments: delta plain swamp, coastal bay/lagoon, or prodelta. For all five lithofacies discussed above, the vertical and lateral lithofacies relationships may help to distinguish among multiple environmental interpretations of each.

After constructing the lithofacies columns for the wells, the next step was to search the well logs for marker horizons which could be correlated from well to well along the stratigraphic cross sections. The correlation markers recognized on the Cerro Prieto well logs represent the tops or bottoms of distinctive depositional units (sands or shales), many of which were identified from a combination of well log curves (particularly SP, gamma-ray, and resistivity). These correlation markers are considered to be approximately time-equivalent stratigraphic horizons. Very few correlation markers were found that could be carried across the field, which is not surprising in view of the deltaic depositional setting. With the correlation markers as a guide, lithofacies correlations were made from well to well. The geometry of the correlation markers suggests that some of the lithofacies correlations essentially parallel time horizons and others clearly cut across time horizons. The lithofacies columns, correlation markers, and lithofacies correlations are given on the four stratigraphic cross-sections (Figures 4-7). The intervals open to production are also shown for reference. In order to emphasize the distribution of relatively thick sand units, lithofacies I, I-II, II, II-III, and III are highlighted on the cross sections (lithofacies I-II and II-III represent transitional or intermediate types).

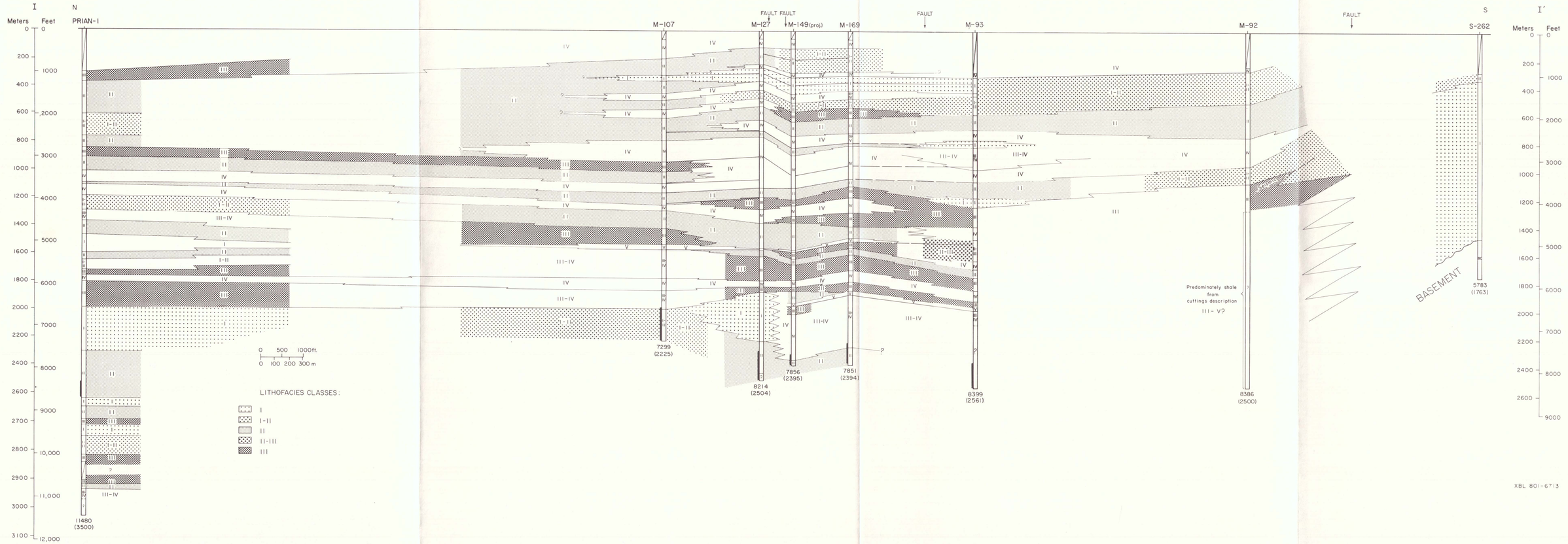


Figure 4. Stratigraphic cross section I-I′ (location in Figure 2).

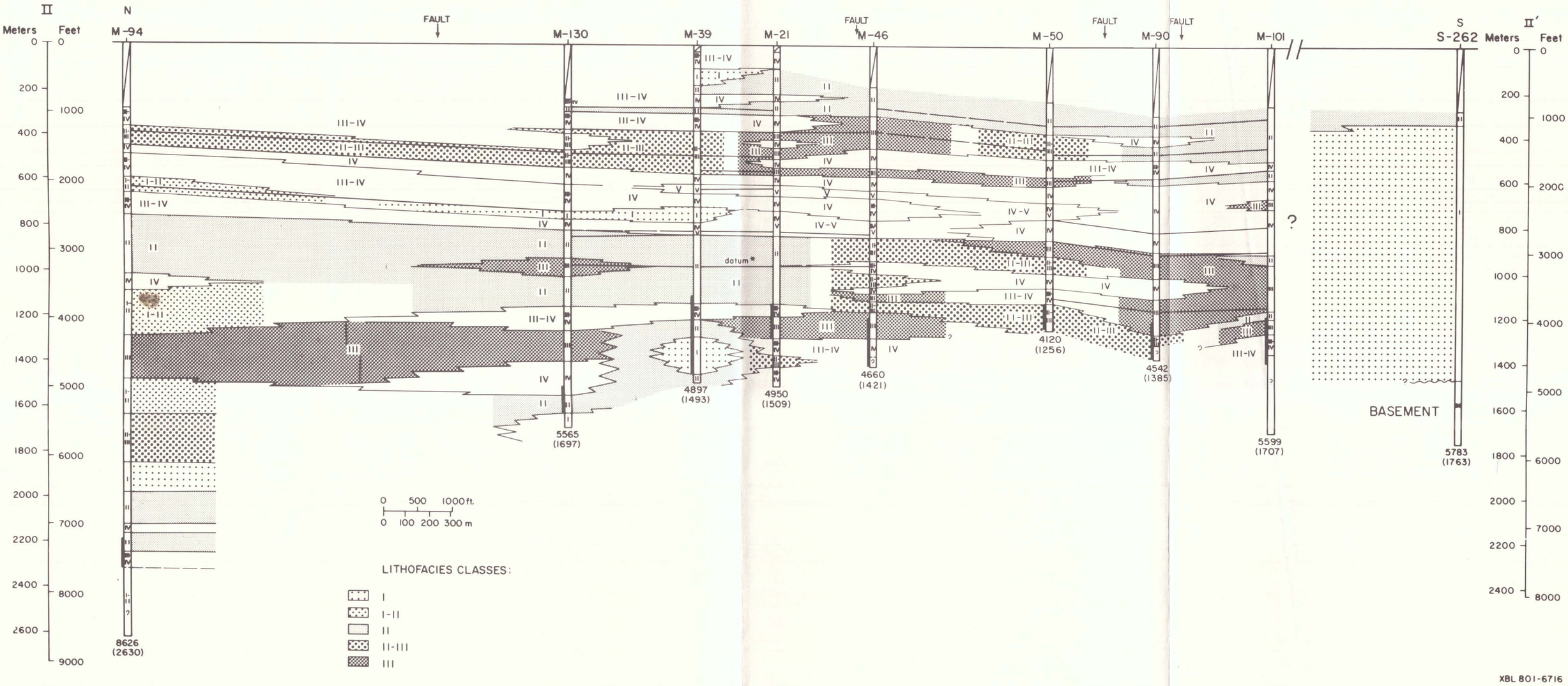


Figure 5. Stratigraphic cross section II-II′ (location in Figure 2).

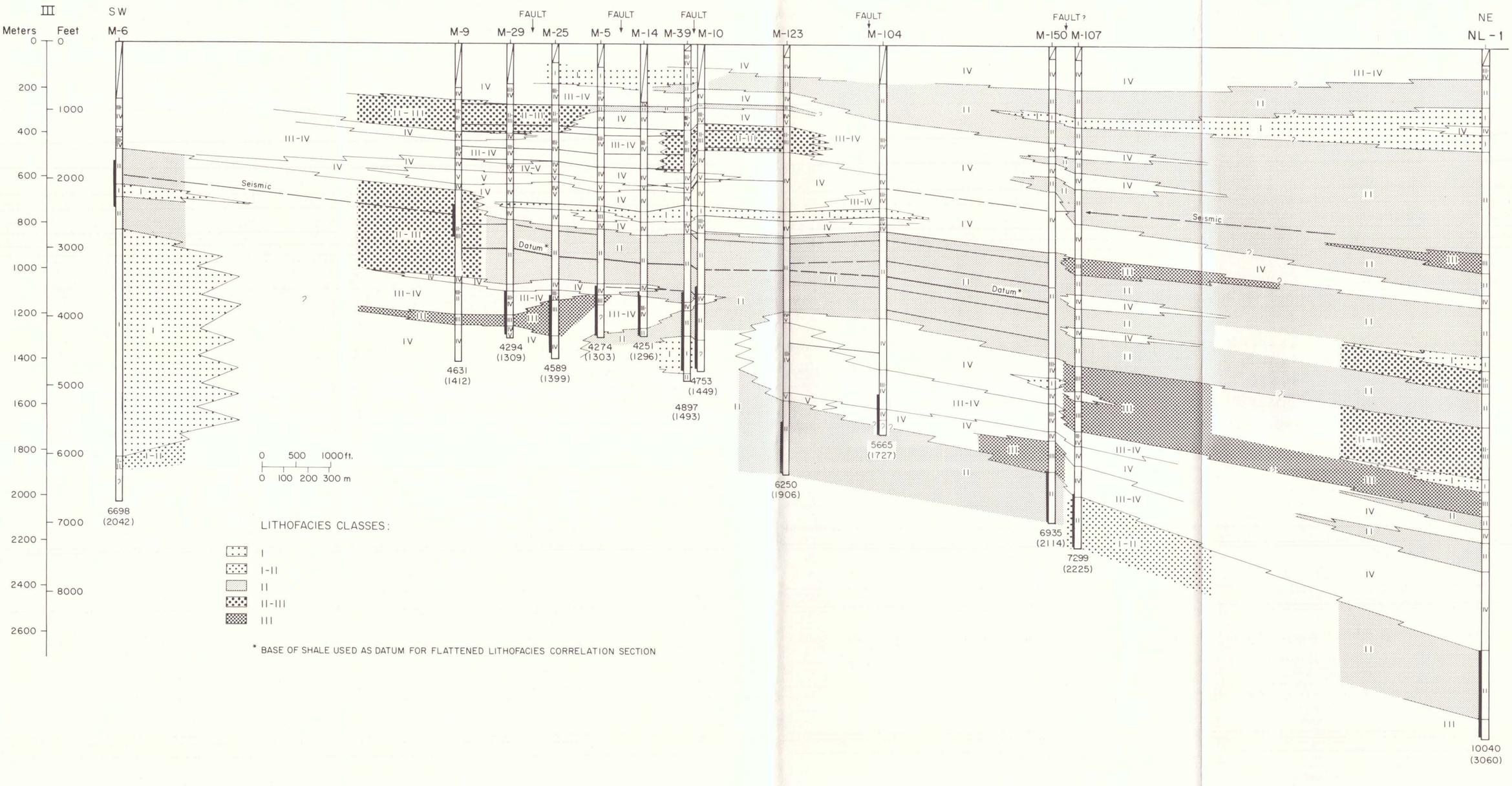


Figure 6. Stratigraphic cross section III-III′ (location in Figure 2).

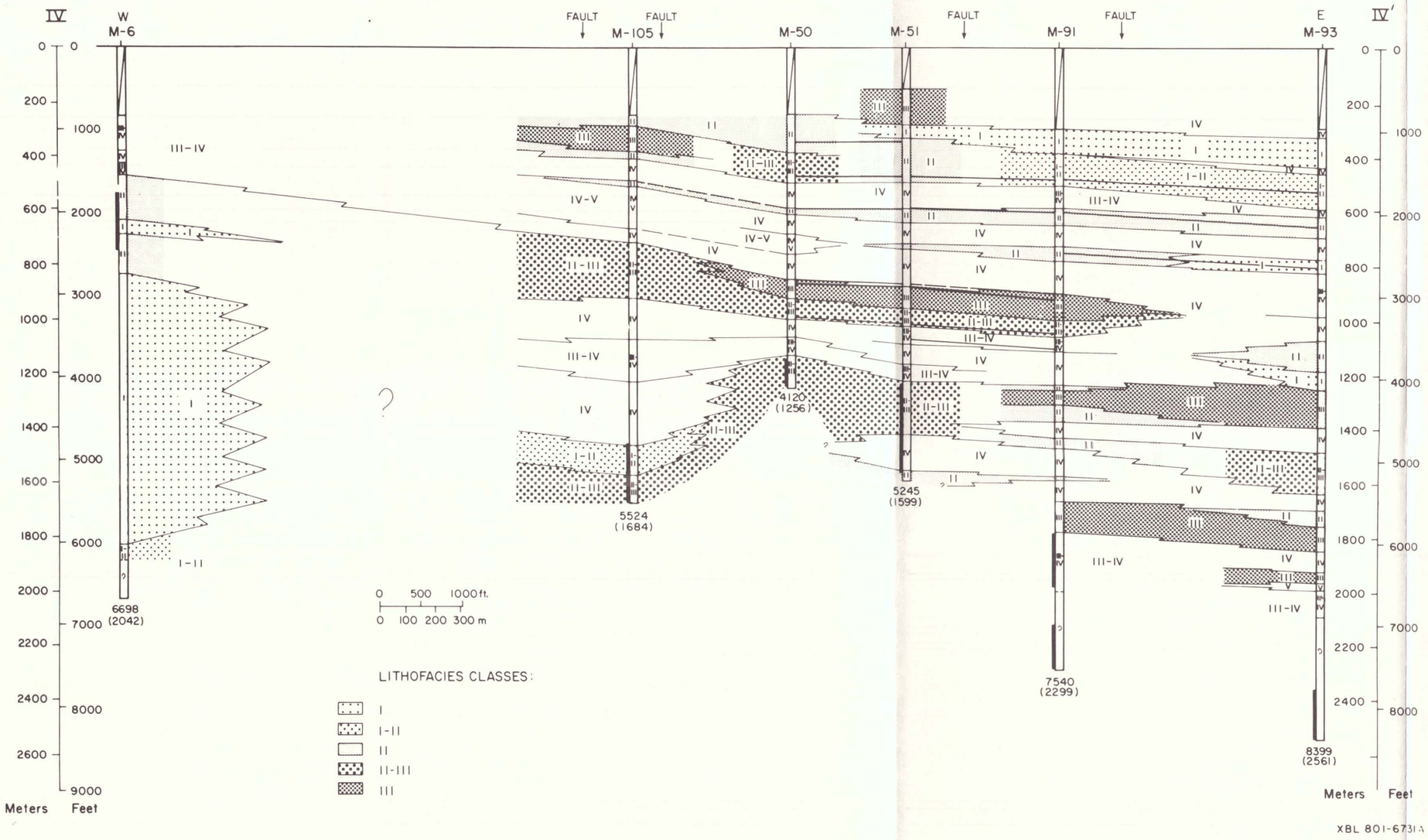


Figure 7. Stratigraphic cross section IV-IV′ (location in Figure 2).

Referring to the stratigraphic cross sections in Figures 4-7, the stratigraphic framework at Cerro Prieto is clearly characterized by complex vertical and lateral variations in lithofacies, which is typical of deltaic deposits. A lithofacies correlation between two wells does not imply continuity of individual sands between the wells. The actual probability of sand continuity within a given lithofacies depends on the depositional environment and the orientation of the line of section with respect to depositonal trends.

To clarify the lithofacies relationships within the main geothermal production zone, the effect of later structure was removed by using the nearest overlying correlation marker with the greatest lateral extent as a datum for restoring the stratigraphic relationships in the underlying section. The restored cross sections, which are given in Figure 8, follow stratigraphic cross sections II-II′ and III-III′ (Figures 5 and 6), but are shorter because of the limited distribution of the datum horizon. The lithofacies vary from I to IV both vertically and laterally within the production zone. The position of Reservoir A (Abril G. and Noble, 1979; Prian C., 1979a,b) is shown on the restored cross-sections where information was available. Even within this "reservoir," the lithofacies vary from I to III-IV. It is clear from Figure 8 that the geothermal production zone is not a uniform reservoir layer overlain by a laterally continuous top-seal of low-permeability strata.

It seems reasonable that the pronounced lithofacies variations illustrated in the stratigraphic cross-sections (Figures 4-7) must significantly influence the movement of hot brines and cold recharge waters and reservoir productivity. Thus, this information should be useful for designing reservoir simulation

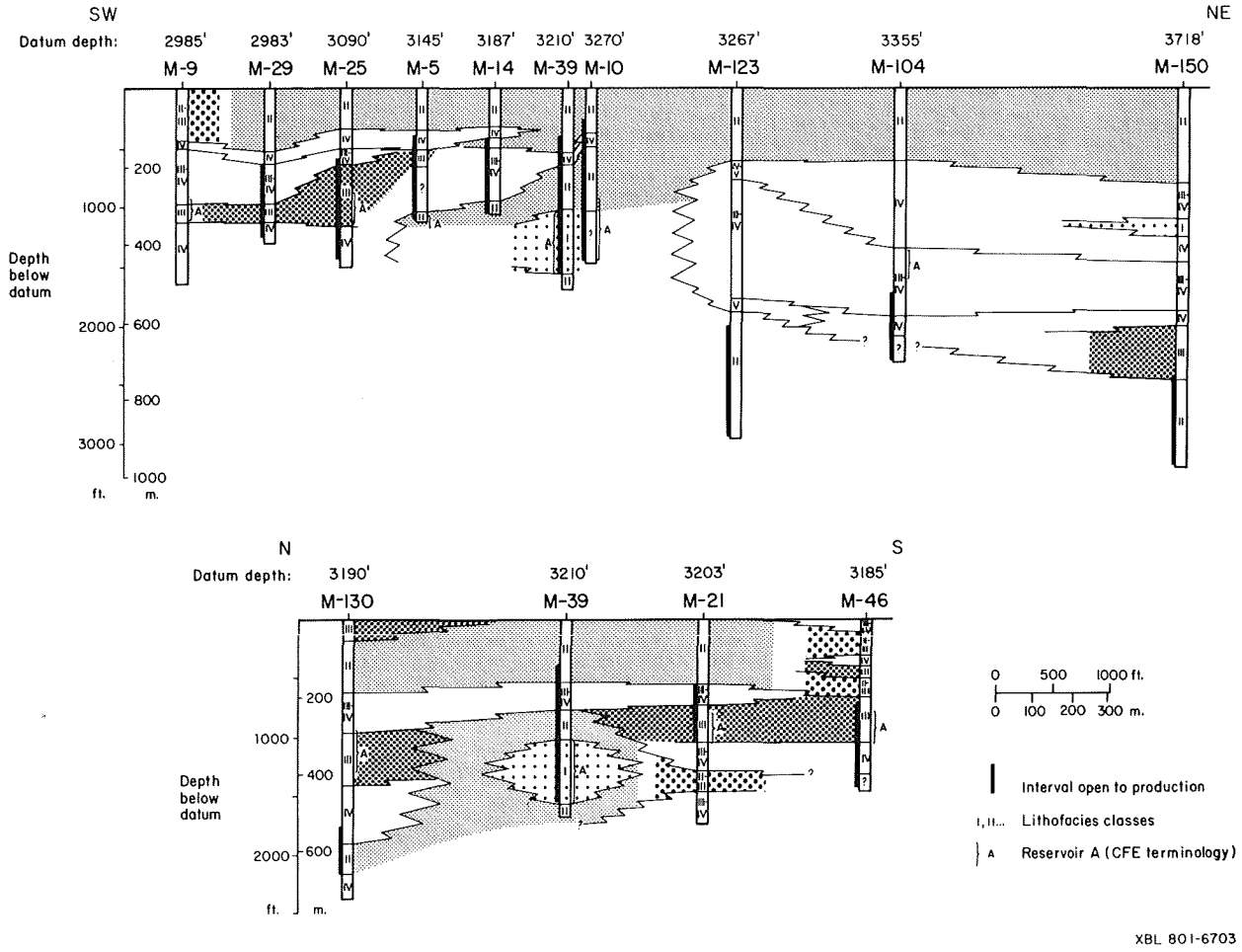


Figure 8. Restored stratigraphic cross sections for the productive level in the older part of the field. The flattened datum is the base of a correlative shale, and the present depths of the datum horizon are given above the wells.

models and for planning and monitoring field development (i.e., production and injection wells).

## 3. DEPOSITIONAL MODEL

As mentioned earlier, the Cerro Prieto field is located near the southwestern margin of the Colorado River delta. There is general agreement that the stratigraphic sequence penetrated in the main producing area represents deltaic deposits and that alluvial fan deposits occur in the subsurface along the western margin of the basin near the mountain front. Between these areas, however, the paleo-depositional environments are not as clear. One of the keys to the problem is the environmental significance of the stratigraphic sequence encountered in wells northwest, west, and south of the main producing area. The deeper part of the section in wells M-96, M-3, M-6, and S-262 is dominated by lithofacies I. Several workers (e.g. Mañon M. et al., 1977) have interpreted the stratigraphic section in the vicinity of these wells as the intertonguing of alluvial fan deposits derived from the Cucapa Range to the west with deltaic deposits derived from the Colorado River. On the other hand, Prian C. (1979a) relates the very thick lithofacies I interval to a major paleochannel on the delta. Various types of data that bear on the interpretation of depositional environments in the Cerro Prieto area will be considered in this section. Several problems with the alternate interpretations above will be discussed, and a new depositional model will be suggested for the deeper part of the section including the main production zone.

### Sandstone Composition

In the Imperial Valley, van de Kamp (1973) found that Colorado

River sands are compositionally distinct from sands derived from the intrusive and metasedimentary rocks of the Peninsular Ranges on the west flank of the basin. The composition of Cerro Prieto sandstones was examined to differentiate sands derived from the Colorado River from sands derived from the Cucapa Range to the west, which is comprised of basically the same rock types as the Peninsular Ranges to the north. To determine sandstone composition quantitatively, a petrographic study was done on thin sections prepared from nine core samples representing seven wells. The cores studied are listed in Table 1. Point counts of 300 to 500 points were made on seven sandstones from six wells.

The sandstone composition data (Table 1) show that the major detrital components are quartz, plagioclase, K-feldspar, and volcanic rock fragments with minor amounts of chert, carbonate, and micas. Quartz is the dominant component comprising 44% to 76% of the solid framework by volume. Feldspars make up 12% to 18% of the framework. As illustrated on the ternary compositional diagram in Figure 9, these sandstones are similar to the Holocene Colorado River sands in van de Kamp (1973) and are considerably less feldspathic than arkosic Holocene sands derived from the Peninsular Ranges on the west flank of the Imperial Valley. Although these thin sections are a small statistical sample of sandstone composition below abou 800 m, the cuttings descriptions by CFE personnel indicate that the petrographic data are representative of the sampled interval. Therefore, it appears that sandstones throughout the Cerro Prieto field area, at least below 800 m, were derived from the same source as the Holocene Colorado River sands, i.e., the Colorado Plateau provenance.

TABLE 1. CERRO PRIETO FIELD SANDSTONE COMPOSITIONS

| | Well Number and Depth (m) | | | | | | |
|---|---|---|---|---|---|---|---|
| | M-6 | M-9 | M-96 | M-96 | NL-1 | M-92 | M-20 |
| | 1910 | 818.5 | 1979 | 1981 | 2735 | 2510 | 915.3 |
| Quartz | 64.3 | 44.0 | 76.0 | 63.0 | 63.2 | 64.0 | 66.7 |
| Plagioclase | 8.9 | 6.7 | 7.0 | 4.7 | 7.2 | 7.0 | 6.0 |
| K-feldspar + perthite | 9.6 | 9.7 | 6.3 | 9.7 | 6.2 | 7.3 | 6.0 |
| Muscovite | tr. | | | | | 0.7 | tr. |
| Biotite | 0.7 | 0.3 | | tr. | | tr. | |
| Chlorite | | | tr. | | tr. | | 0.3 |
| Illite + clays | | 1.0 | 0.3 | 1.0 | 12.1 | | 1.0 |
| Heavy & opaque | 0.7 | | 0.3 | tr. | 0.2 | tr. | 1.0 |
| Siltstone & shale R.F. | 0.5 | | 0.3 | | | 1.7 | 1.3 |
| Volcanic R.F. | 9.3 | 7.7 | 3.7 | 11.7 | 2.5 | 13.0 | 10.7 |
| Chert | 1.4 | 1.0 | 2.7 | 1.3 | 1.2 | 0.3 | 1.0 |
| Metamorphic R.F. | | | | | | | tr. |
| Granitic R.F. | 0.7 | 0.6 | | | | | |
| Glauconite | | | | tr. | | | tr. |
| Epidote | 0.3 | | | | 7.4 | | 0.3 |
| Carbonate | 2.1 | 29.0 | 3.3 | 8.3 | | 5.7 | 5.7 |
| Isotropic mineral | 1.4 | | | | | | |
| Organic matter | | | | | | 0.3 | |
| Grain Size | m | m | f-m | m-c | f | f | f-m |
| Sorting | w | w | w | m-w | w | w | w |
| Porosity (%) | 23.5 | 18.0 | 22.3 | 14.2 | 21.5 | 28.6 | 23.7 |
| Permeability (md) | 22.0 | 47.0 | 4.8 | 2.5 | 18.1 | 4.9 | 33.0 |

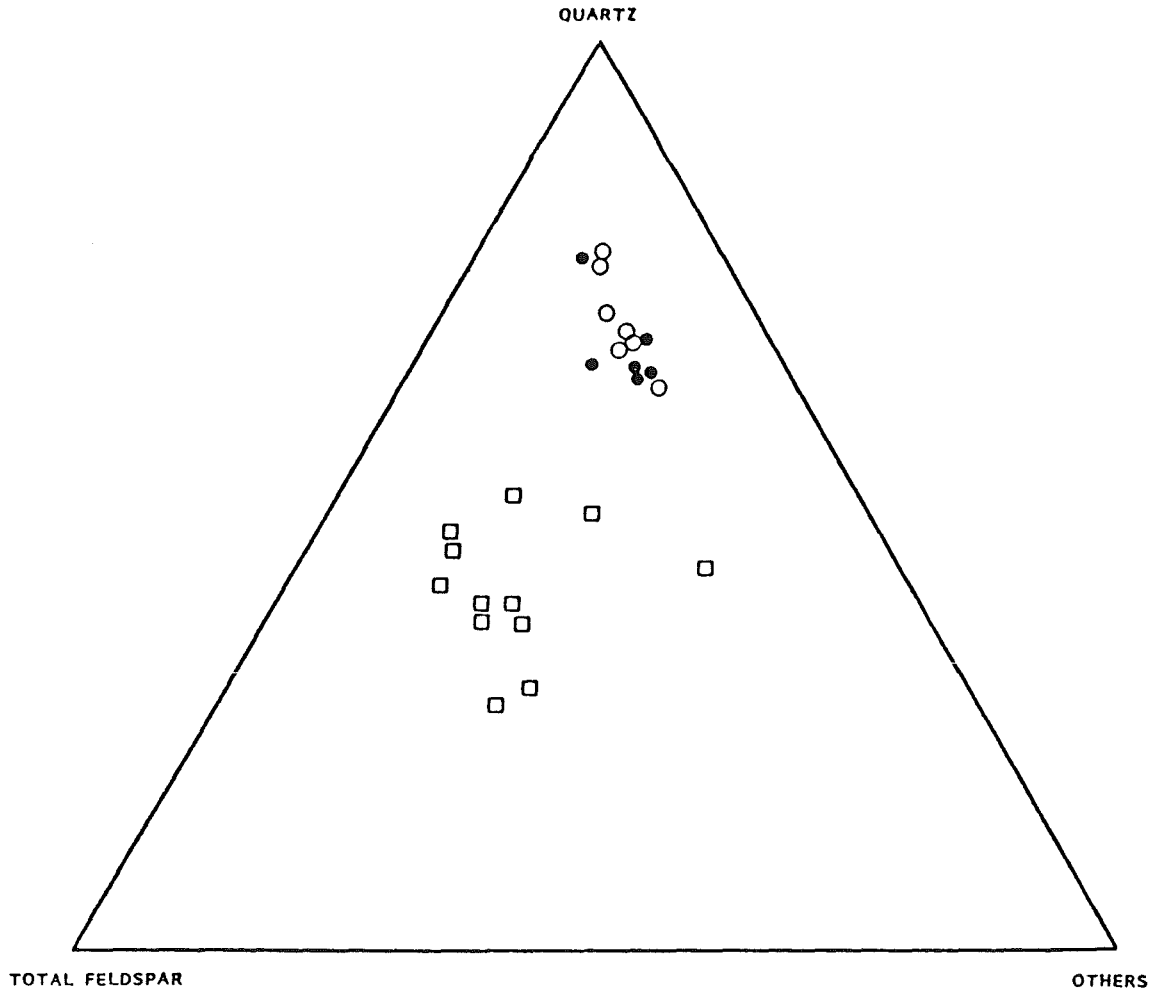


XBL 808-11541

Figure 9. Composition diagram comparing sandstones from subsurface at Cerro Prieto (dots), Holocene Colorado River sands (circles), and arkosic Holocene sands derived from Salton Trough margin (squares). The samples from Cerro Prieto and the Colorado River are similar, suggesting they had a common source.

Pore Water Salinities

Pore water salinities for sands were interpreted from well log data to provide clues to depositional environments (fresh-water, transitional, or marine). In well NL-1 east of the field, sands in the unconsolidated to semi-consolidated portion of the section commonly exhibit anomalous SP (suppressed or reversed), high resistivities (5 to 20 ohm-m on the deep investigation curve), and "normal" densities. These characteristics indicate low pore-water salinities, i.e., fresh-water sands. Good SP development and lower resistivities indicate more saline sands. The gamma-ray log is useful for recognizing sands where the SP response is anomalous, while the sonic or density log normally discriminates high-resistivity zones due to induration (anomalously low transit time or high density) or gas saturation (anomalously high transit time or low density). Thus, a suite of well logs is necessary for interpreting salinity changes with confidence.

Based on the well log data, the percentage of fresh-water sands gradually decreases in a westerly direction across the producing area as shown on the cross section in Figure 10, which corresponds to cross-section III-III′ in Figure 6. In well M-6 on the west edge of the field, only one thin fresh water sand was noted (at about 900 ft or 274 m), although others may be present in the interval above 830 ft (253 m) for which logs are not available.

This lateral salinity gradient suggests a transition from an upper delta plain environment east of the Cerro Prieto field to a marine environment west of the field. This transitional environment interpretation is supported by the geochemical analysis of the reservoir fluids by Truesdell et al.

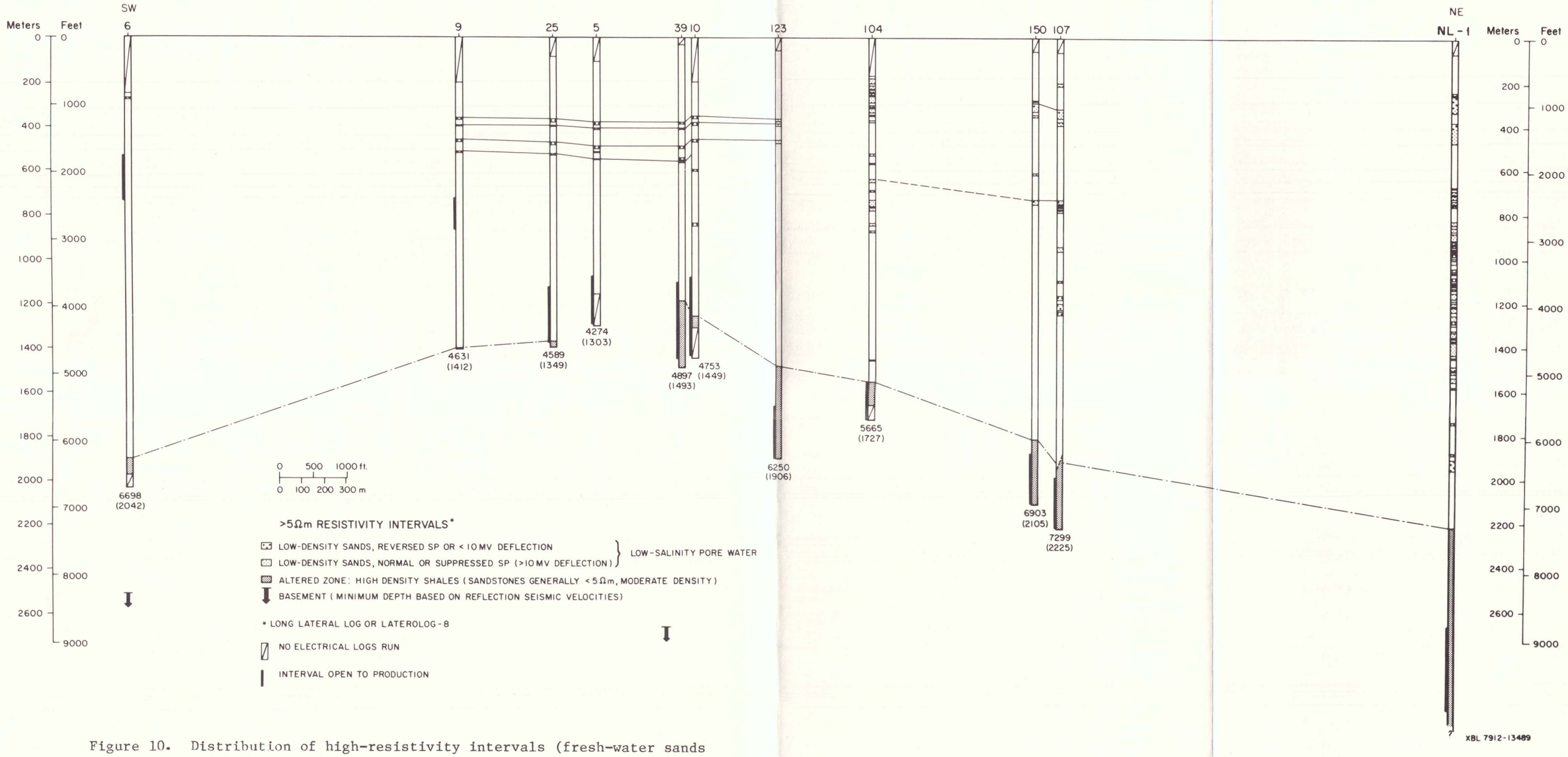


Figure 10. Distribution of high-resistivity intervals (fresh-water sands and hydrothermally altered zone) along cross section III-III′.

(1979). Their data indicate mixing of Colorado River water with sea water (or possibly lagoonal or estuarine water).

The salinity data are not consistent with a continuous alluvial fan wedge from the mountain front to the west side of the field. If the thick lithofacies I sequences in S-262, M-6, M-3, and M-96 represented distal alluvial fan facies, low-salinity sands should be characteristic of the interval in these wells. This is clearly not the case.

If the predominantly sand interval in these wells represented a major paleochannel on the delta (actually, stacked distributary channels, because of the great thickness) as suggested by Prian C. (1979a), delta plain sediments would be expected to the west. In that case, salinities on the west side of the field should not be significantly different from salinities on the east side. Hence, this environmental interpretation is also not consistent with the lateral salinity gradient.

Surface resistivity surveys (e.g., section E-E′ located in Figure 2, and in Wilt et al., 1979) showed decreasing resistivity from northeast to southwest above the production zone, which may be explained by the lateral salinity gradient interpreted from well log data. Other evidence will be discussed below supporting a depositional environment interpretation for the salinity gradient. Variations in salinity due to depositional environment should be taken into account before interpreting the distribution of hot brines and cold, low-salinity recharge waters from resistivity data.

## Seismic Reflection Patterns

Seismic reflection patterns can be useful for interpreting lithofacies variations and depositional environments. Before discussing the seismic data from the Cerro Prieto area, a brief review of basic principles is in order.

Seismic reflections are produced by the interaction of a down-going seismic signal with acoustic impedance (velocity times density) contrasts in the subsurface. Generally, these so-called primary reflections parallel bedding (depositional surfaces) and thus define the geometry of the subsurface strata. Coherent seismic events may also represent multiple reflections; diffractions (normally hyperbolic events caused by lateral terminations of reflectors, inhomogeneities, or tight curvature); reflections from out of the plane of the seismic profile ("side-energy"); or source-generated surface waves. These unwanted events often can be recognized by their discordant geometry, but not always. Multiples that may be generated within the stratigraphic section and at the surface may not be recognizable. Velocity analysis data (velocity spectra) are also useful for discriminating primary reflections from unwanted events (noise).

The principal characteristics of seismic reflections for stratigraphic interpretation are amplitude, spacing (frequency), lateral continuity, lateral waveform variations, and geometry. Although it is beyond the scope of this report to discuss these parameters in detail, it must be noted that they also depend on factors unrelated to stratigraphy, such as source signal characteristics, recording parameters, processing of the data, various types of noise, surface statics, multiple reflections, structure, and pore fluid variations. However, from a careful analysis of seismic sections, inferences about stratigraphy and depositional environments can be derived from the combined reflection attributes, if the data are not too noisy.

The portion of the D-D′ seismic profile extending from well M-9 to the southwest is given in Figure 11. Primary reflections are obscured in places

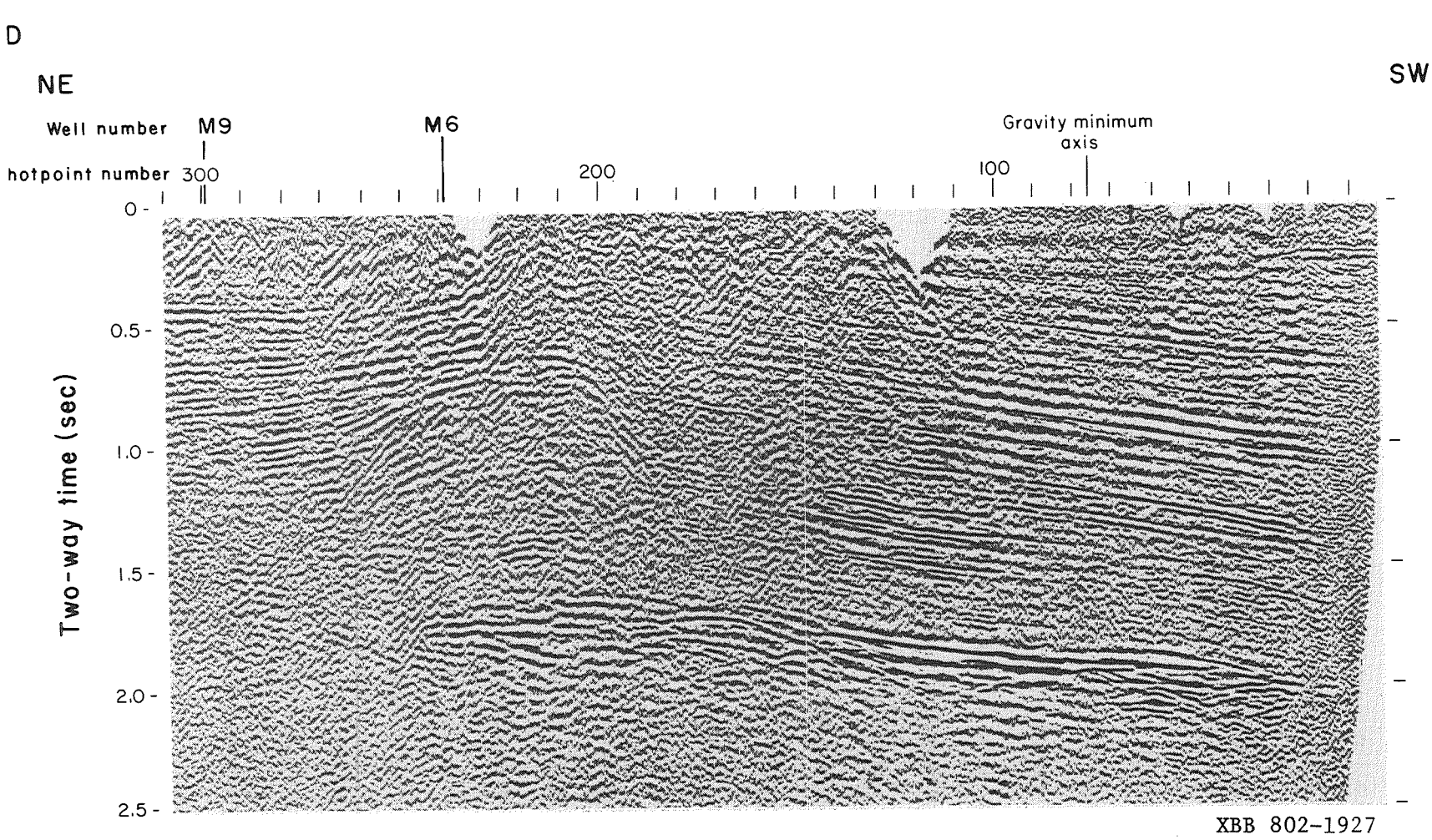


Figure 11. Portion of reflection seismic profile D-D′ from near well M-9 to the southwest illustrating apparent volcanic layer underlying interpreted marine strata southwest of the Colorado delta.

by (1) random noise, (2) steeply inclined, low velocity events, which are related to surface waves, and (3) fault disruptions and diffractions (just southwest of M-6). Only minimal processing of the data was done; namely, band-pass filtering (16/24/60/80 Hz) and stacking based on widely spaced velocity analyses. With additional processing, it is conceivable that the seismic section could have been "cleaned up." Looking through the noise, we see closely spaced parallel reflections southwest of shotpoint 180 extending from near the surface down to the strong reflection below about 1.7 seconds. Since many of the reflections are truncated at the end of the line, the lateral reflection continuity may be much greater than seen on the seismic section. Because of the variable data quality and the processing used, reflection amplitude and waveform variations may not represent stratigraphic changes. The seismic reflection pattern from just southwest of M-6 to the end of the D-D′ profile suggests an alternating lithologic sequence with good lateral continuity of the lithologic units.

In contrast, at well M-6 there is downward loss of reflections. Comparing the reflection pattern to the stratigraphic sequence in the well (refer to cross-section III-III′ in Figure 6), it is apparent that the well developed reflections in the shallower part of the section correspond to an alternation of lithofacies types (I, II, III-IV and IV), while the reflection-poor zone corresponds to the thick lithofacies I interval. Surface wave noise, faulting, and possible diffraction energy also interfere with any primary reflections in the reflection-poor zone; but it is clear from the well log data that very few primaries would be expected in this zone. Since the strong reflections below the reflection-poor zone were not penetrated by M-6, their stratigraphic significance is unknown.

Another example of the relationship between the stratigraphic sequence and seismic reflections is on seismic profile A-A′ at M-93 (Figure 12). The abundant reflections seen on the section correspond to a complex alternation of lithofacies types (from I to IV). The loss of reflections below about 1.9 seconds is probably related to hydrothermal alteration, which will be discussed in detail later.

The relationships between stratigraphic sequence and seismic reflection patterns seen at M-6 and M-93, which we observed in a variety of sedimentary basins, support our interpretation of the reflection pattern southwest of M-6: i.e., alternating lithologic sequence with good lateral continuity of lithologic units. We cannot conclude that a unique depositional environment exists, particularly without more seismic coverage to determine the geographic extent of this reflection pattern. For a deltaic setting, some possibilities are coastal bays in a river-dominated delta, tidal flats (lower delta plain) in a tide- or wave/tide-dominated delta, or low-energy delta front to prodelta.

In spite of the environmental ambiguity of the reflection pattern southwest of M-6, it seems clear that the thick lithofacies I interval in M-6 is not continuous with the basin margin alluvial fan wedge to the southwest, but is separated by an area of alternating sand and shale deposition. This is consistent with the sandstone composition and pore water salinity data. The lateral salinity gradient described earlier suggests that a delta front to marine environment would be more likely than coastal-deltaic or lower delta plain.

Combining well data and seismic reflection patterns, an attempt was made to map the distribution of the thick lithofacies I encountered in

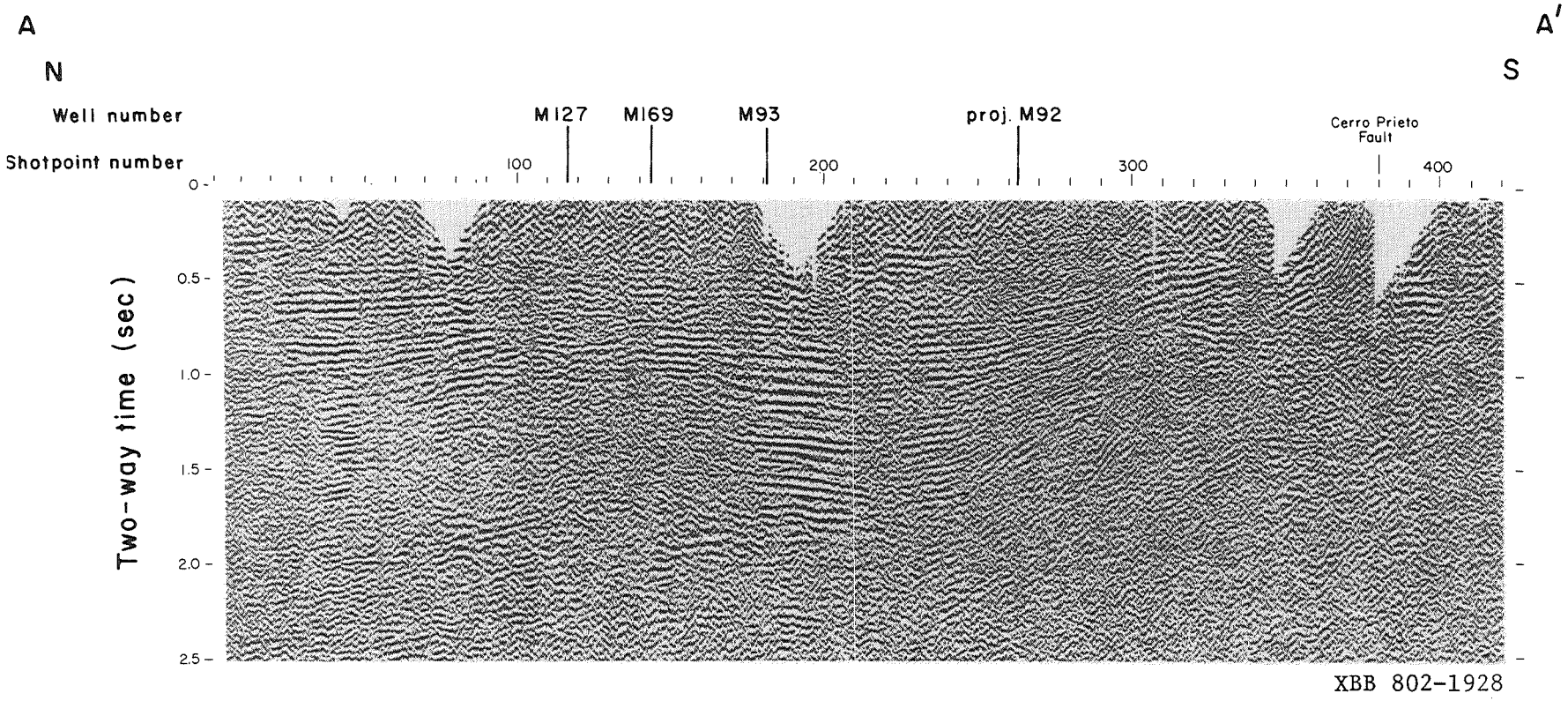


Figure 12. Portion of reflection seismic profile A-A′ from just north of the field to the vicinity of well S-262.

S-262, M-6, M-3, and M-96. The extent of this lithofacies in a transverse direction is best defined in the vicinity of M-6. Although the seismic reflection pattern immediately southwest of M-6 is obscured by faulting, the position of the southwest limit of lithofacies I can be rather closely approximated. Northeast of M-6, however, seismic interpretation of the lithofacies boundary is not possible because of the disruption of depositional reflections by the cross-cutting hydrothermal alteration zone (discussed later). Because the equivalent interval in M-9 is represented by lithofacies III, III-IV, and IV, the boundary is arbitrarily placed midway between M-6 and M-9.

The northeastern boundary of lithofacies I in the vicinity of S-262 was interpreted from the seismic reflection pattern on the nearby A-A′ seismic profile (Figure 12). The reflection-poor zone below about 0.65 seconds to the south of shotpoint 305 in Figure 12 probably corresponds to the lithofacies I interval in S-262, although faulting may be partially responsible for the disappearance of reflections. This pattern is in sharp contrast to the closely spaced parallel reflections north of shotpoint 290. The pattern correlates with a complex alternating stratigraphic sequence in M-92 (refer to cross-section I-I′ in Figure 4), located about 360 m west of the profile. The reflection pattern north of shotpoint 290 continues to the M-93 well mentioned above. It was not possible to recognize a southwest boundary in this area due to seismic data quality deterioration and the lack of well control.

A possible extension of the northeast boundary of the lithofacies I belt to the southeast was based on a tentative interpretation of reflection patterns on seismic profile E-E′. Because of shallow data gaps and poor

data quality, this interpretation is less reliable than the interpretation of profiles D-D′ and A-A′.

No seismic profiles are available to define the lithofacies I boundaries near M-3 and M-96. East and northeast of M-3, the boundary can only be approximated based on well control. A thick lithofacies I sequence was not found in M-9, M-11, M-114, or M-94, but it is not clear whether the lithofacies I belt includes M-7 and Q-757 because of the relatively shallow depths of these wells. No well control is available to define the southwest boundary near M-3 or either boundary near M-96.

Based on the above interpretation of well and seismic data, the thick lithofacies I sequence occurs in an arcuate belt extending from northwest to south of the field. This is illustrated on the depositional environment map (Figure 16) at the end of Section 3 (Depositional Model). The environmental significance of this lithofacies belt will be discussed below.

Present Physiography

The present physiography of the Colorado delta suggests that the distributary channels trended from northwesterly to southerly during the late Cenozoic evolution of the delta, but, in the vicinity of the field, were dominantly southwesterly which is roughly normal to the thick lithofacies I belt. It would be a remarkable coincidence if the four wells (M-96, M-3, M-6, and S-262) all penetrated separate stationary distributary channel sequences. Furthermore, since deltas are characterized by shifting distributaries, the great thickness of lithofacies I in these wells ($\geq$ 3280 ft or 1000 m) seems inconsistent with a composite distributary channel interpretation.

Rather, the position and trend of the arcuate lithofacies I belt suggests a coastal-deltaic environment. The apparent lateral continuity of this lithofacies belt indicates strong wave and/or tidal influence (as opposed to a river-dominated birdfoot delta). A variety of coastal genetic sand types are present in such deltas, including some or all of the following: distributary channel or estuary, eolian, beach/shoreface, tidal channel, and tidal bar/shoal. Thus the thick lithofacies I sequence may be a composite of many genetic sand types. Grain size variations noted in cores from fine-grained sand to conglomeratic coarse-grained sand and complex dip patterns on dipmeter logs (variable dip azimuths and magnitudes) support such a composite sequence, although it was not possible to break the sequence down into genetic units with the available data. Closely spaced cores would be necessary for a detailed genetic interpretation.

Based on the present topography southwest of the field, the late Quaternary alluvial fans on the flank of the Cucapa Range do not appear to extend into the area underlain by closely spaced, parallel, laterally continuous reflections southwest of the thick lithofacies I belt (seismic profiles D-D′ and E-E′). The gravity data (Figure 13) and seismic profile E-E′ (Figure 14) suggest that the main basin boundary fault is buried in the subsurface approximately 2.4 km to the east of the present mountain front, which is ~~toward the basin~~ basinward of the limit of the "modern" fans. Buried mountain fronts have also been observed in the valleys of the Great Basin in Nevada (e.g., Foster, 1979). Nonetheless, the dimensions of the late Quaternary fans suggest that even fans related to the buried mountain front would not have extended across the area of the reflection pattern described above (Figure 15). This is consistent with the interpretation given

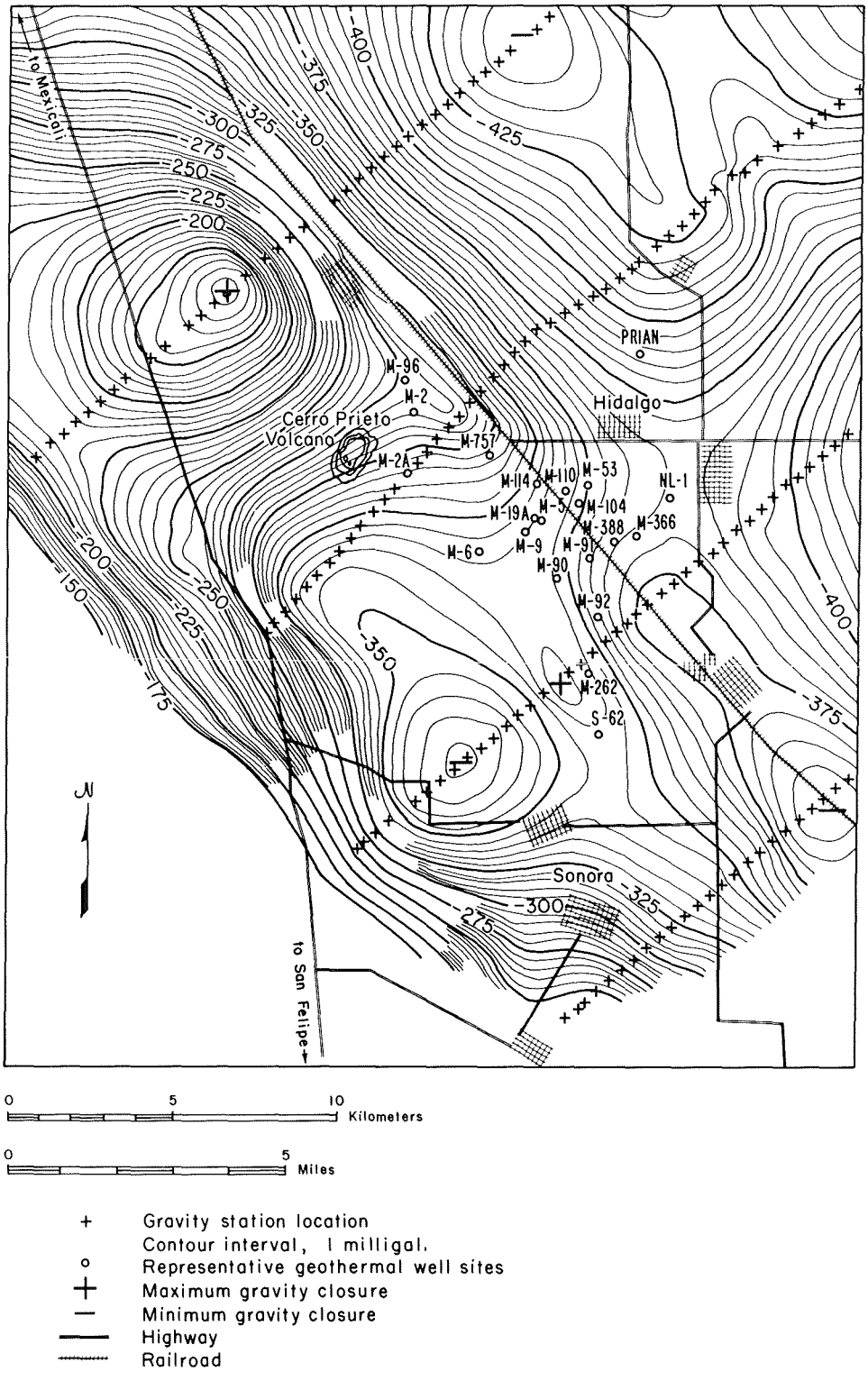


Figure 13. Bouguer gravity anomaly map of Cerro Prieto area (Razo M. and Fonseca L., 1978).

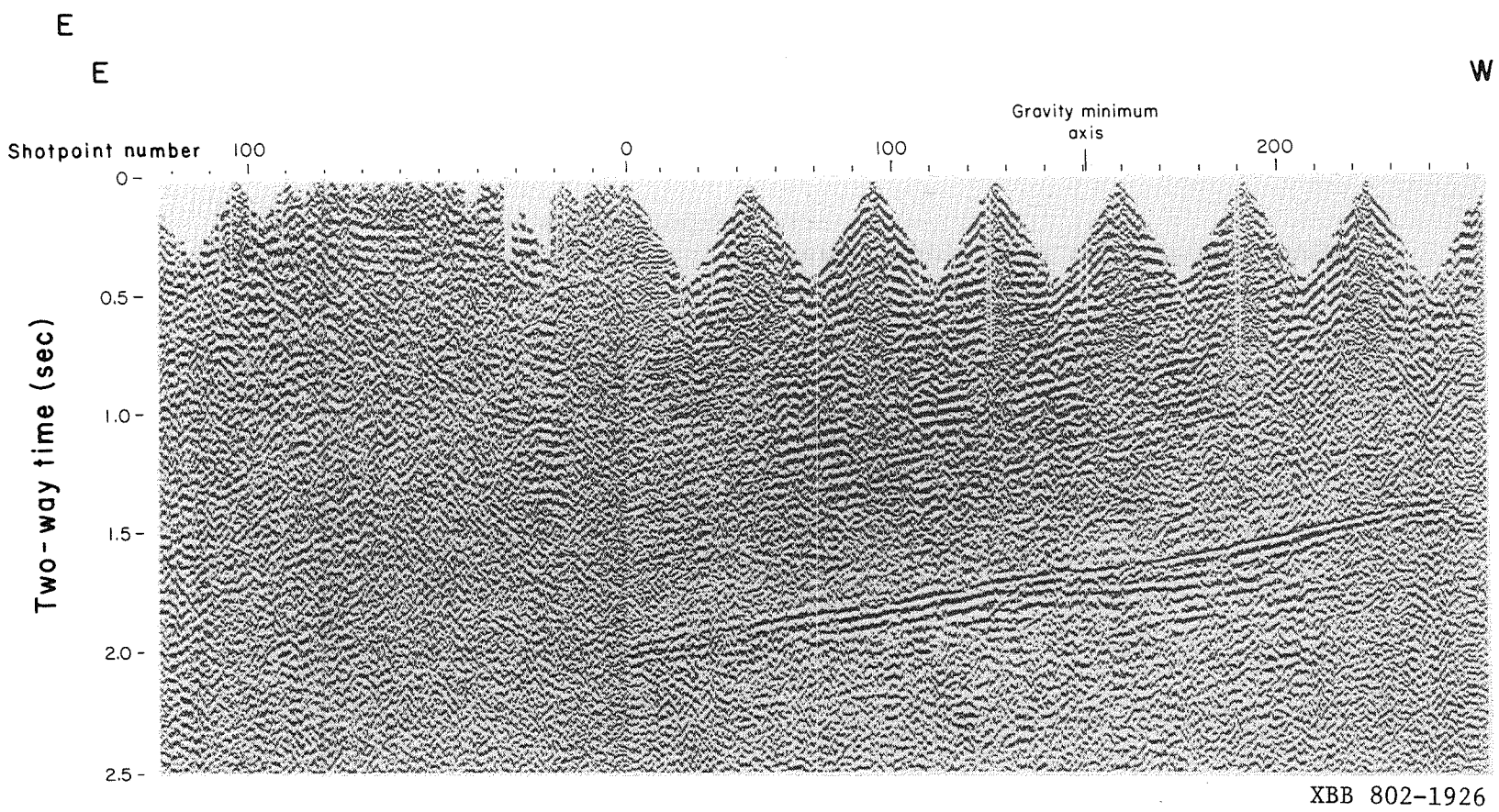


Figure 14. Southwest portion of reflection seismic profile E-E′ illustrating buried mountain front (basin boundary fault) and apparent volcanic layering underlying interpreted marine strata southwest of the Colorado delta.

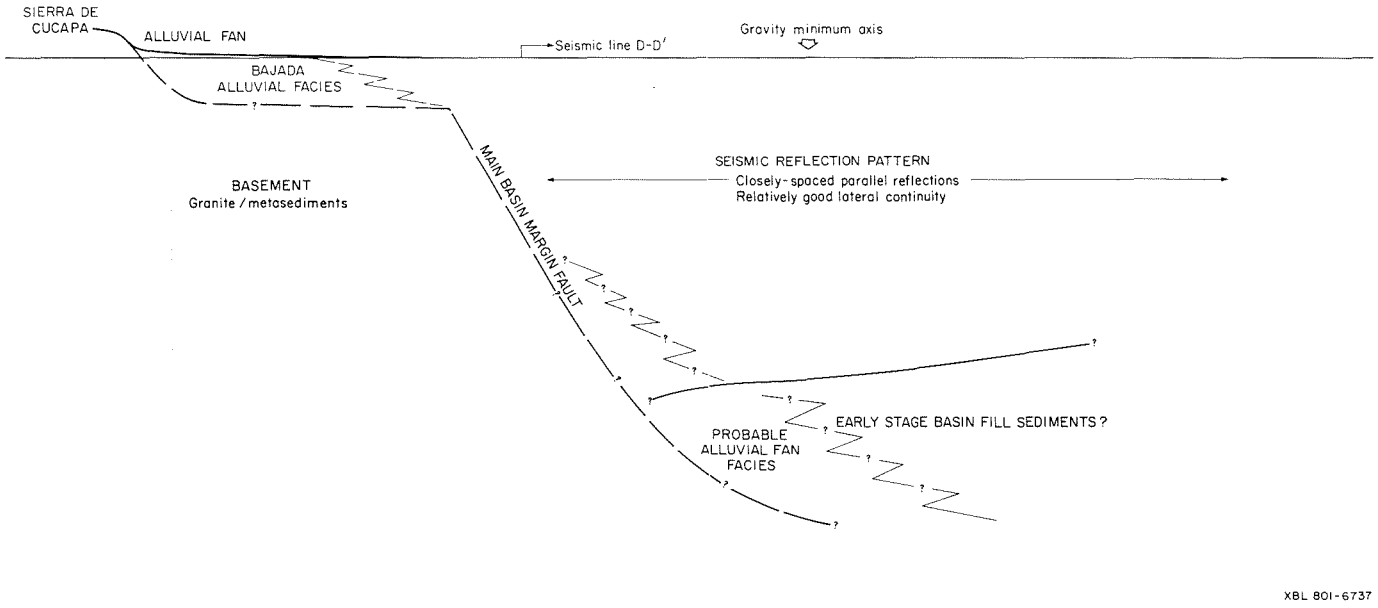


Figure 15. Basin fill facies from the Cerro Prieto field to the Cucapa Range and basin margin configuration.

earlier that this reflection pattern represents an area of marine deposition separating the Colorado delta from the basin margin alluvial fans.

Imperial Valley Depositional Record

According to Woodard (1974), intermittent shallow marine deposition continued until middle Pleistocene in the western part of the Imperial Valley. This implies that there was an intermittent connection to the Gulf of California west of the Colorado delta until middle Pleistocene which is probably represented by the area between the basin margin alluvial fans and the thick lithofacies I belt.

Considering the strong tidal currents at the head of the present Gulf of California, it is reasonable to assume that strong longitudinal tidal currents were present in the narrow remnant of the paleo-sea-arm southwest of the Colorado delta. Such currents would have redistributed sand supplied by the distributaries along the delta front, thus contributing to the development of a continuous sand belt. Shoreward and longshore transport by wave energy (longshore drift) may also have been a factor. To build up such a thick sequence of lithofacies I, deposition and subsidence must have been in balance.

The thick lithofacies I sequence in M-6, for example, is overlain by about 2700 ft or 823 m of interbedded sands and shales. The salinities of the sands, indicated by electrical log curves and the color of the fine-grained sediments from the cuttings descriptions, suggest an upward gradation from shallow marine/nearshore to nonmarine. This sequence probably corresponds to the late Pleistocene infill of the connecting "estuary."

Synthesis

A generalized map of the depositional environments is shown in Figure 16 for the deeper part of the section (including the main productive zone) in the Cerro Prieto area. This interpretation is based on the lithofacies relationships, sandstone composition, pore water salinities, seismic reflection patterns, present physiography, and regional basin history.

## 4. STRUCTURE

Granitic rocks were penetrated in three wells (M-96, M-3, and S-262), which suggests that the basement underlying the Cerro Prieto area corresponds to the Upper Cretaceous granitic and metasedimentary rocks outcropping in the Cucapa Range to the west and southwest. The subsurface structure is characterized by complex block faulting of the basement and overlying sedimentary section.

Fault maps have been produced by several investigators based on different types of data: i.e., well log correlations (Abril and Noble, 1979, Prian C., 1979a; Puente C. and de la Peña L., 1979); aerial photos and seismic refraction (Puente C., and de la Peña L., 1979); gravity (Razo M. et al., 1979); and seismicity (Albores L. et al., 1979). One widely held view is that there are two principal fault systems: northeast-southwest trending normal faults forming horsts and grabens in the field area bounded by en echelon northwest-southeast trending strike-slip faults to the northeast and southwest (Figure 17). An analogy has been made to pull-apart basins (possibly spreading centers) between en echelon transform faults in the Gulf of California (Elders et al., 1972).

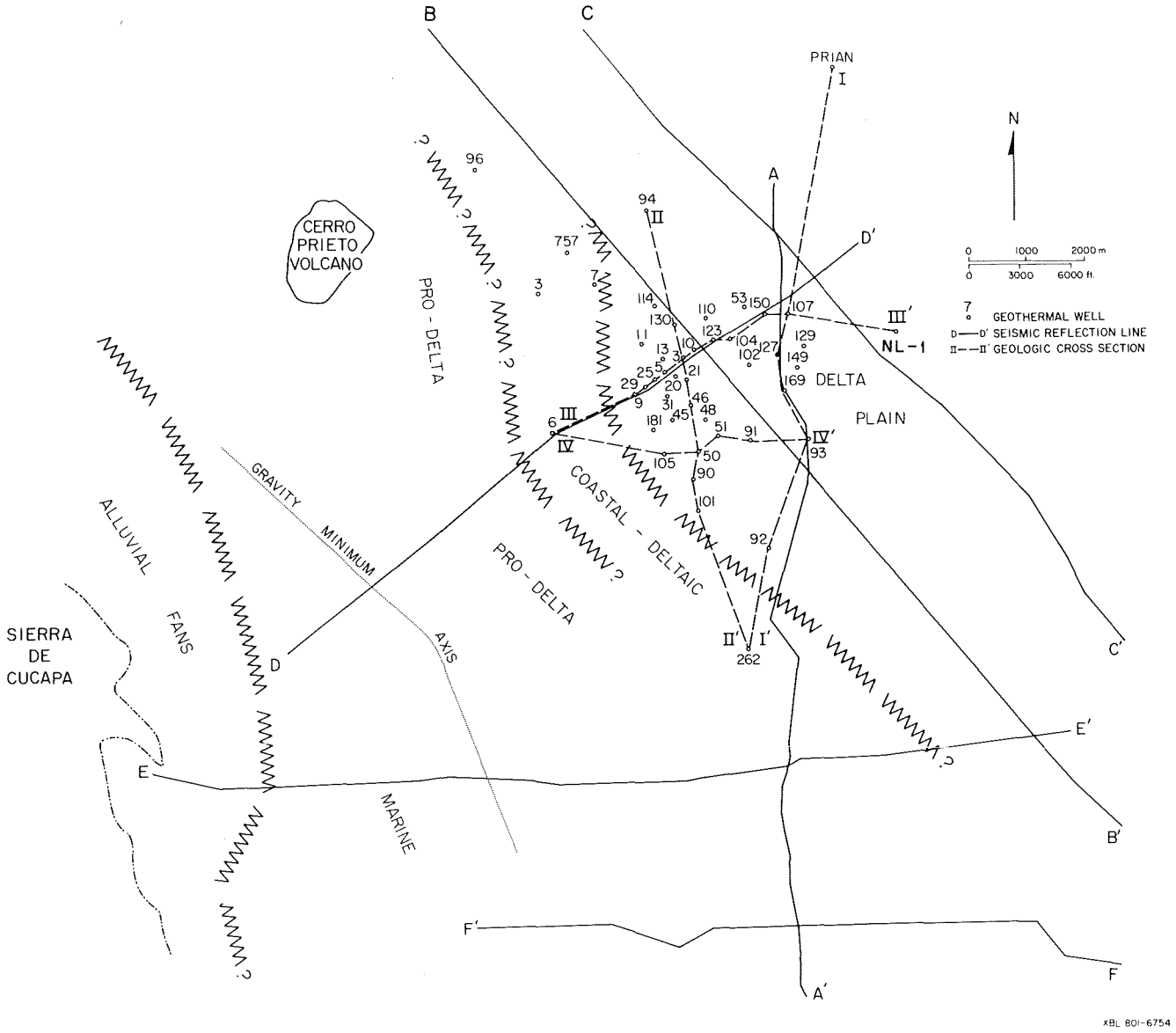


Figure 16. Generalized map of depositional environments for the deeper part of the section (including the main productive zone).

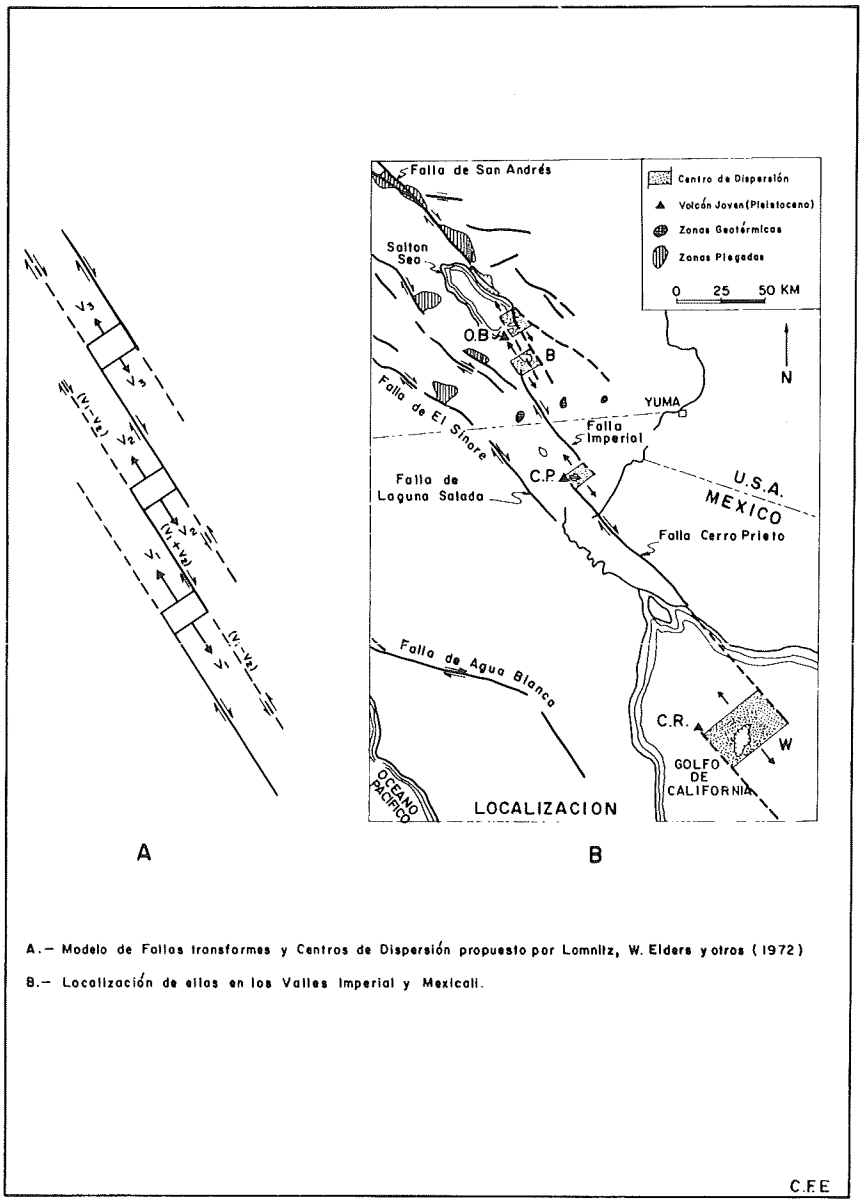


A.– Modelo de Fallas transformes y Centros de Dispersión propuesto por Lomnitz, W. Elders y otros (1972)

B.– Localización de ellos en los Valles Imperial y Mexicali.

XBL 7811-12843

Figure 17. Regional tectonics (Elders et al., 1972). The spreading center indicated at Cerro Prieto is the area of northeast-southwest trending extensional faults.

## Fault Interpretation

In this study, a fault map (Figure 18) was produced based on an integrated interpretation of well log correlations, linear surface features (mainly drainage patterns), thermal springs, seismic reflection and refraction profiles, and gravity and magnetic maps. Linear surface features are indicated as faults on the map only where there is supporting evidence of displacement from other data. It is not known whether the other surface linears represent major faults or minor faults with insignificant displacement.

Some of the faults interpreted by other workers were recognized and some were not. There may be many more faults present than shown in Figure 18. Faults could be seen on the reflection seismic sections for which the fault trends could not be determined, due to the lack of supporting evidence away from the seismic profiles. Moreover, some apparent offsets of correlation markers between well pairs could not be mapped as faults with the subsurface control used in the study (46 wells out of 64 were correlated). If all the wells at Cerro Prieto had been correlated, undoubtedly more faults would have been mapped.

Three principal classes of faults were identified based on the timing of fault displacements of the basin fill which were recognized from offsets of correlation markers. The three classes are: (1) older faults offsetting the deeper part of the section only; (2) reactivated older faults with a smaller offset or reversed sense of offset above some horizon relative to the offset below that horizon (the reversed offset case may represent two separate nearby faults); and (3) young faults offsetting the entire section. An example of the first type of fault displacement between wells M-50 and M-90 is illustrated in Figure 5, the second type between wells M-39 and M-10 is

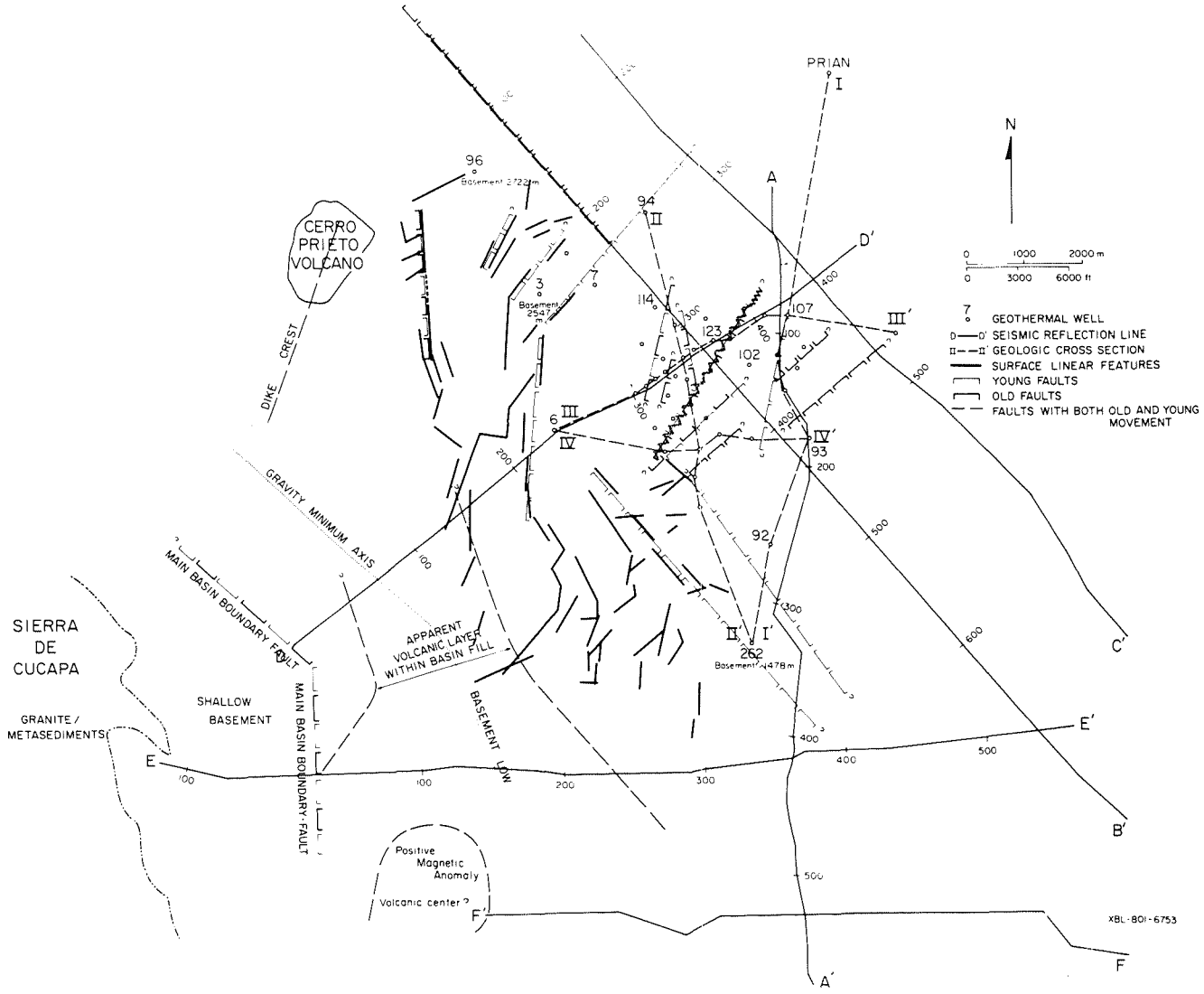


Figure 18. Faults and surface linears, apparent distribution of volcanic layer and possible volcanic center southwest of the field, and gravity minimum axis in the same area.

shown in Figure 6, and the third type between wells M-90 and M-101 appears in Figure 5. These fault classes are identified on the fault map in Figure 18.

This classification of faults does not imply that there were only two periods of faulting since the formation of the basin in the Miocene. The well log correlations indicate that the older faults are not all time-equivalent (refer to the stratigraphic cross-sections in Figures 4-7). Furthermore, earlier faulting events may be recorded in the older part of the basin fill not penetrated by the wells at Cerro Prieto. Although the surface linears indicate very young fault movements, at least some of these features may be reactivated older faults. Any of the faults recognized in the basin fill may represent reactivation of the initial faulting of the basement in the Miocene. It is not clear how many periods of faulting have occurred, but there may have been intermittent faulting in this area since the Miocene.

The northeast-southwest trending zigzag line on the fault map (Figure 18), extending from just east of M-53 to just west of M-105, represents the southeastward termination of several distinctive sands in the shallow part of the section which exhibit anomalous log response patterns (suppressed or reversed SP and relatively high resistivities). These sands were discussed in Section 2 (Lithofacies Analysis). This lateral discontinuity may be a strike-slip fault because well log correlations suggest that (1) there is no significant vertical displacement along some parts of this line, and (2) where there is vertical displacement, it may be related to faults with a different trend.

Only dip-slip fault displacement could be recognized from the geophysical data and well-log correlations. Consequently, although the faults are shown as dip-slip faults on the map in Figure 18, there may be a significant lateral-slip component in some cases (oblique-slip faults).

The faulting in the Cerro Prieto area appears more complex than indicated in previous papers, in terms of fault trends and history of fault movements. In addition to the northeast-southwest and northwest-southeast fault trends which have been emphasized in earlier fault interpretations, north-south and north northeast-south southwest trends are also prominent on the fault map.

It has been suggested that the faults in the field are growth faults because of increasing offset of correlation markers with depth (Razo M., personal communication, 1979). This offset pattern is illustrated by most of the faults shown in the cross sections in Abril G. and Noble (1979). Many of the earlier correlations are questionable, however, due to pronounced lateral stratigraphic changes (refer to the stratigraphic cross sections in Figures 4-7 of this report) and cross-cutting hydrothermal alteration effects (e.g., the A/B boundary discussed in the Lithofacies Analysis section). Well-log correlations in this study, however, suggested distinct episodes of fault displacement for most of the interpreted faults rather than continuous growth.

## Basement Structure

Using available data, it is very difficult to define basement structure in the Cerro Prieto area. Only three wells penetrated basement (M-3, M-96, and S-262), at depths of 2722 m, 2547 m, and 1478 m, respectively; but nearby wells indicate abrupt changes in depth to basement. Basement interpretation

from geophysical data is confused by anomalies within the basin fill. Geophysical data coverage is another limiting factor. Various problems in interpreting basement structure in this area from geophysical data are discussed below, followed by an interpretation of the major basement structural features.

The seismic reflection data are not tied to any of the basement tests. An apparent basement reflection was recognized only in a few places south and southeast of the field (e.g., on profile G-G′ in Figure 19). Part of the structural confusion on this seismic section is apparently due to reflected energy coming from out of the plane of the section. A strong westerly dipping reflection southwest of the field (profiles D-D′ and E-E′ in Figures 11 and 14) has been interpreted as basement by Fonseca L. and Razo M. (1979). This reflection is interpreted in this study as a volcanic layer underlain by sedimentary strata for the following reasons:

1. Apparent primary reflections can be seen beneath ~~the record of~~ this event, especially on profile D-D′ which is less noisy than E-E′.
2. It appears to grade laterally into lower amplitude reflections on profile D-D′ rather than terminate by faulting.
3. Just northeast of this strong reflection on profile D-D′, the stacking (normal moveout) velocities indicate sedimentary interval velocities for the interval which appears to be laterally equivalent to the apparent primary reflections seen beneath the "basement" reflection.
4. The magnetic map (Figure 20) suggests a uniform westerly dip for the magnetic basement in the area of this strong reflection, which also has a monoclinal westerly dip. The

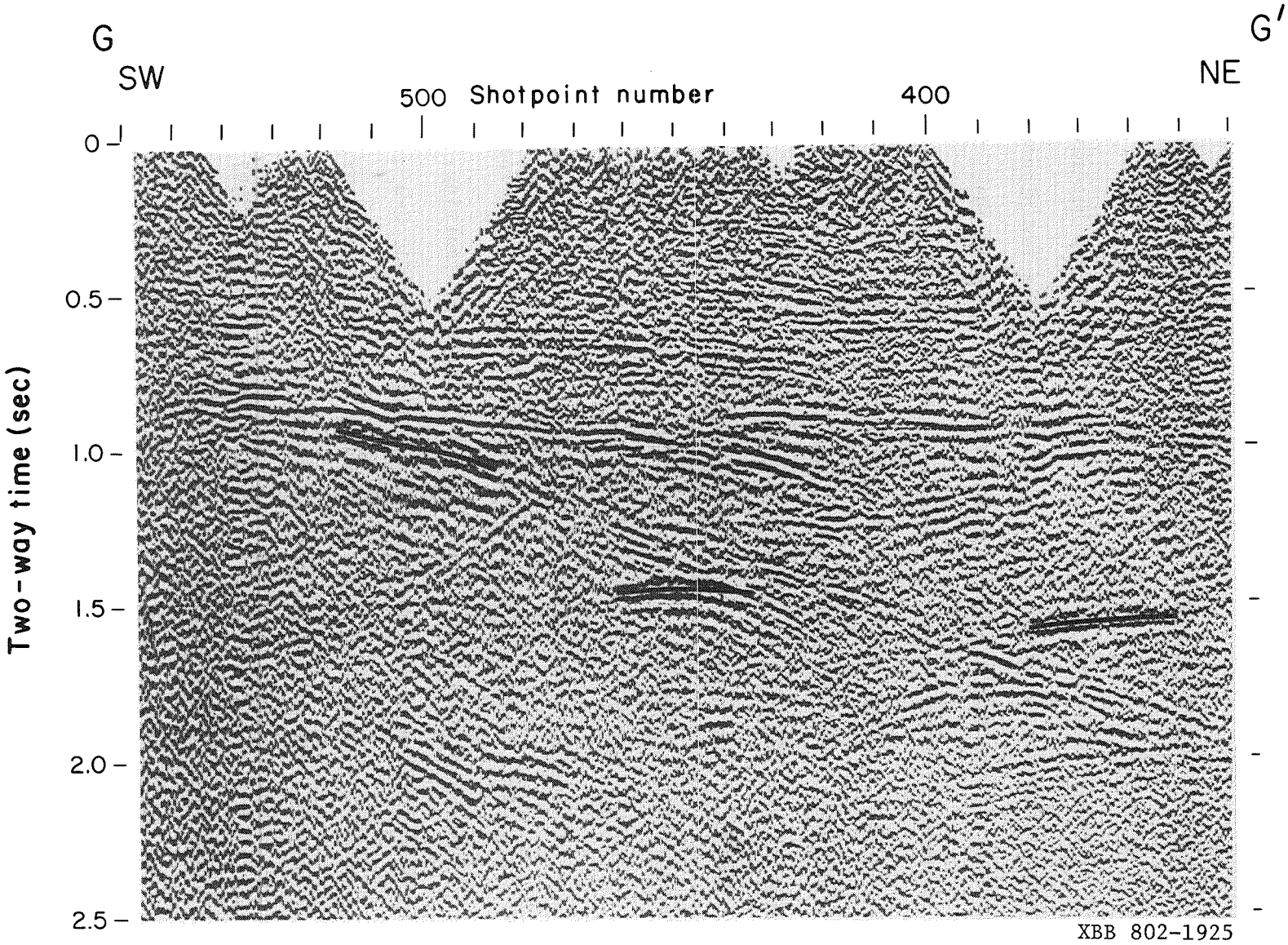


Figure 19. Portion of reflection seismic profile G–G′ illustrating apparent basement reflection which was only recognized in a few places south and southeast of the field.

Bouguer gravity map (Figure 13), however, shows a gravity minimum axis crossing profiles D-D′ and E-E′ in this area suggesting that the sedimentary section thickens and then thins in a westerly direction across the area of the strong reflection, which seems to require sedimentary strata below this supposed basement reflection.

The distribution of this apparent volcanic layer was estimated by extrapolating away from the reflection limits on profile D-D′ by following the trend of the magnetic contours. The estimated distribution is consistent with the apparent limits of this reflection on profile E-E′. A small positive magnetic anomaly occurs within this area south of profile E-E′ along the interpreted basin boundary fault zone (based on gravity and seismic reflection profile E-E′). This anomaly may represent the volcanic center responsible for the postulated volcanic layer (Figure 18).

A possible interpretation of the basement structure southwest of the field is given in ~~the in~~ Figure 15. In this area, the gravity data seem to define the basement structure better than the magnetic or reflection seismic data (compare Figures 11, 13, and 20). However, the occurrence of high-density sedimentary rocks above basement in other areas suggests that gravity data may not always provide accurate depths to basement throughout the region. For example, in the Imperial Valley, ~~the coincidence~~ ~~of~~ seven of the known geothermal anomalies coincide with positive gravity anomalies, which have been explained by densification of the sediments during hydrothermal alteration (Smith, 1979). This may not be the sole reason for the high gravity reading over part of the Cerro Prieto field (see Figure 13) because of a more complex geology, including the alteration history, which will be considered later.

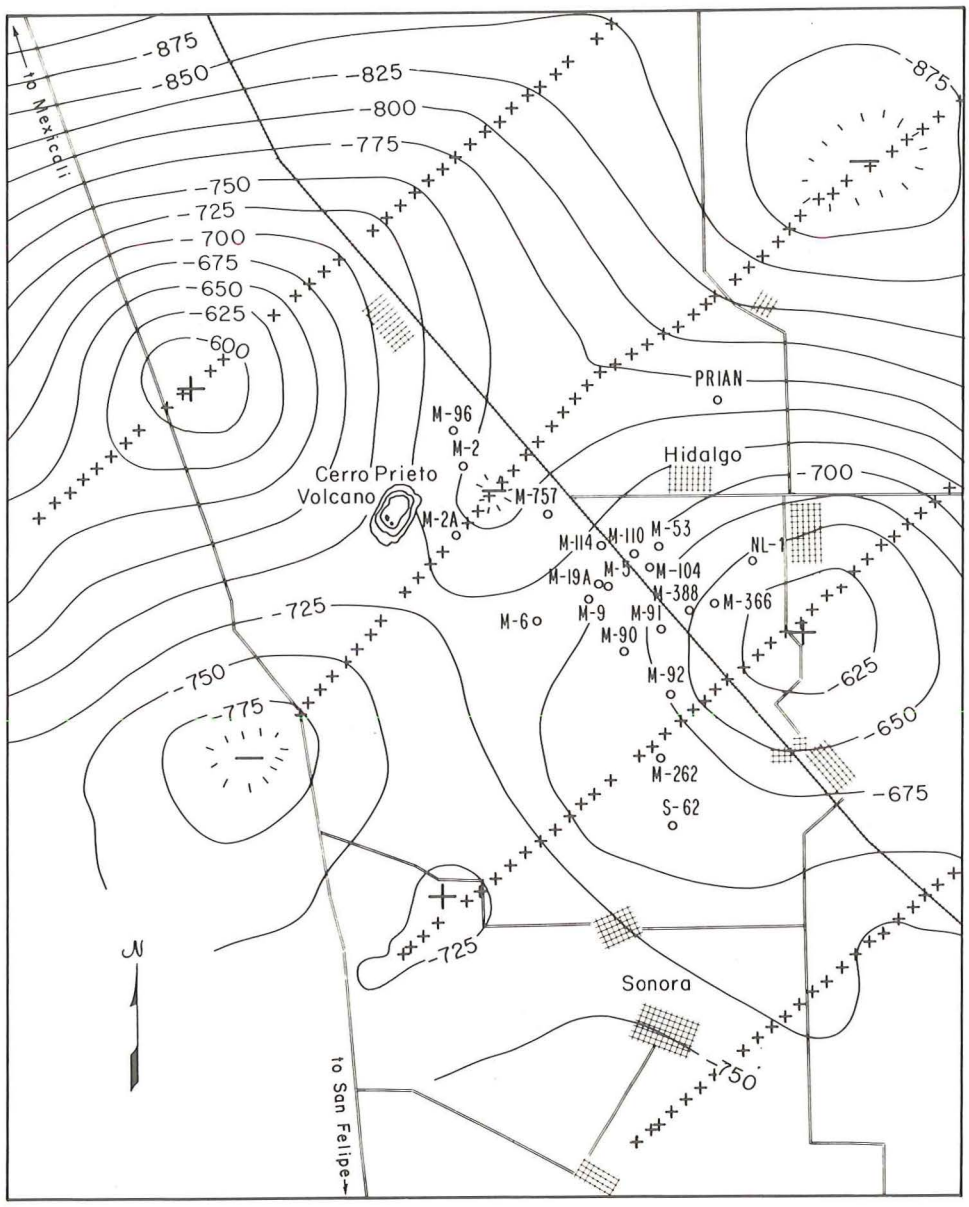


Figure 20. Magnetic anomaly map of Cerro Prieto area (Razo and Fonseca, 1978).

Northwest of the producing area, however, wells M-96 and Q-757 are on a narrow northwest-southeast trending gravity high (Figure 13). The gravity field on this ridge-like anomaly is approximately 55 mgal higher than the field at well S-262, which intersects basement at a depth 1244 m shallower than basement at M-96 (Figure 13). This discrepancy appears to be due to densified sediments above basement. In both M-96 and Q-757, especially in Q-757, the sediments show a more rapid increase in density with depth than in most of the other Cerro Prieto wells. The interval from about 800-1730 ft (244-527 m) in Q-757 is particularly anomalous with sandstone densities ranging from about 2.25-2.45, which corresponds to a porosity range of about 24%-12%. This interval was described as dominantly quartzite by CFE personnel based on cuttings. A petrographic examination of a thin section from a core taken at 271 to 280 m depth revealed a well-cemented quartzose sandstone with no carbonate and very little clay. If the thin section is representative of the high-density interval, the porosity indicated by the density log is probably mainly secondary solution porosity. So in this area of densified sediments, a basement interpretation before drilling based on gravity would be too shallow.

Seismic refraction data probably provide the most reliable geophysical definition of basement, but unfortunately, in an area of complex block faulting, refraction data coverage and its limited spatial resolution generally are not sufficient for mapping basement structure in any detail. Because of the structural complexity and local occurrence of densified sediments and magnetic igneous rocks above basement (volcanics, sills, and/or dikes) in the Cerro Prieto region, interpretation of basement structure requires integration of gravity, magnetic, reflection, and refraction data. The

data coverage and data quality, however, do not allow us to do much more than interpret the major basement structural features as discussed below.

Both the magnetic and Bouguer gravity maps (Figures 13 and 20) suggest that the basement penetrated by S-262 is on a northwest-southeast trending fault-bounded basement high (horst). The surface expression of the Cerro Prieto fault on the southwest flank (alignment of linear streams, ponds, and thermal springs), seismicity data, and well log correlations from M-90 to M-101 suggest that this basement high is a very young feature.

The negative magnetic anomaly between M-3 and M-96, which crosses the high-gravity ridge discussed above, implies a basement low between these two basement penetrations (Figures 13 and 20). The gravity map suggests that the basement deepens to the east, southeast, and south away from M-3. A young northeast-southwest trending fault between M-3 and M-7 was interpreted from the alignment of a surface linear and an apparently young fault on reflection profile B-B′. Surface linears with a similar trend between M-3 and M-96 suggest that M-3 is on a northeast trending horst separated from the M-96 basement high by a graben (Figure 18). This basement horst and graben structure also seems to be very young, but in contrast to the S-262 horst, the bounding faults are apparently now aseismic (refer to seismicity data in Albores L. et al., 1979).

Another major basement fault was recognized by several workers just east of the Cerro Prieto volcano. Gravity, seismic refraction, and resistivity surveys (Majer et al., 1979; Razo M. et al., 1979; and Wilt et al., 1979) indicate a large westerly downward displacement. The observed displacement coincides with a north-south trending set of surface linears, thus establishing the trend of the fault.

The faulting may be complex in the producing area, but the gravity map (Figure 13) indicates a general deepening of the basement in a southeasterly direction across the field. Although a basement reflection cannot be seen beneath the field, the seismic reflection profiles suggest a relatively deep basement. There does not seem to be any convincing geophysical evidence for a basement horst underlying the field as suggested by various workers in the past.

The positive magnetic anomaly southeast of the field, where the gravity indicates a deep basement, suggests the presence of volcanics and/or dikes and sills within the basin fill (Figures 13 and 20). A reflection-poor zone can be seen on seismic profile C-C′ across this magnetic anomaly. This interpretation was apparently confirmed by recent drilling which encountered diabase in well NL-1 at a depth of about 6500 ft (2000 m) which has been interpreted as a dike/sill complex by CFE personnel (Goldstein, 1980, oral commun.).

## 5. HYDROTHERMAL ALTERATION

### Induration of Sediments

Puente C. and de la Peña L. (1979) divided the stratigraphic section into two major units based on well samples (principally cuttings)--Lithologic Unit A and Unit B. The principal difference between these two units is the degree of consolidation or induration. Thus, the A/B "contact" represents the transition from unconsolidated and semiconsolidated to consolidated. Elders et al. (1978, p. 13) related a high degree of induration to cementation or metamorphic changes and concluded that the A/B boundary "may not be a depositional boundary within the geothermal reservoir." The stratigraphic correlations in our study indicate that the A/B boundary

is not a stratigraphic marker horizon, but an induration boundary that cuts across the sedimentary strata, suggesting localized post-depositional alteration. This relationship is illustrated in Figure 21 for the four cross sections discussed in the lithofacies analysis section. A dome-like configuration can be seen for the induration boundary with the shallowest part coincident with the older producing area (e.g., wells M-5, M-9, M-10, M-14, M-21, M-25, M-39, and M-46). The well-log correlation markers on the cross sections clearly show that the induration boundary does not parallel the strata (seismic reflection correlations are given where well log correlation markers were lacking).

Well Log Evidence

Density logs were examined to determine the effect on rock densities of the change in consolidation at the A/B boundary noted in the well cuttings. A marked increase in shale densities was generally observed at the top of the indurated zone as illustrated by the close correspondence between the depth below which shale densities exceed 2.4 and the A/B boundary on the cross sections in Figure 21. A map of the depth to this shale density level is given in Figure 22.

In addition to shale "densification," electrical logs indicate that induration also produced a marked increase in shale resistivity, but at a greater depth, as shown in Figure 21 by the depth below which shale resistivities exceed 5 ohm-m. The general configuration of the top of the high-resistivity shales is similar to that of the A/B boundary. Figure 23 is a map of the depth to this shale resistivity level. Note the similarity of the two maps. The rock properties of the sandstones are anomalous and will be discussed later.

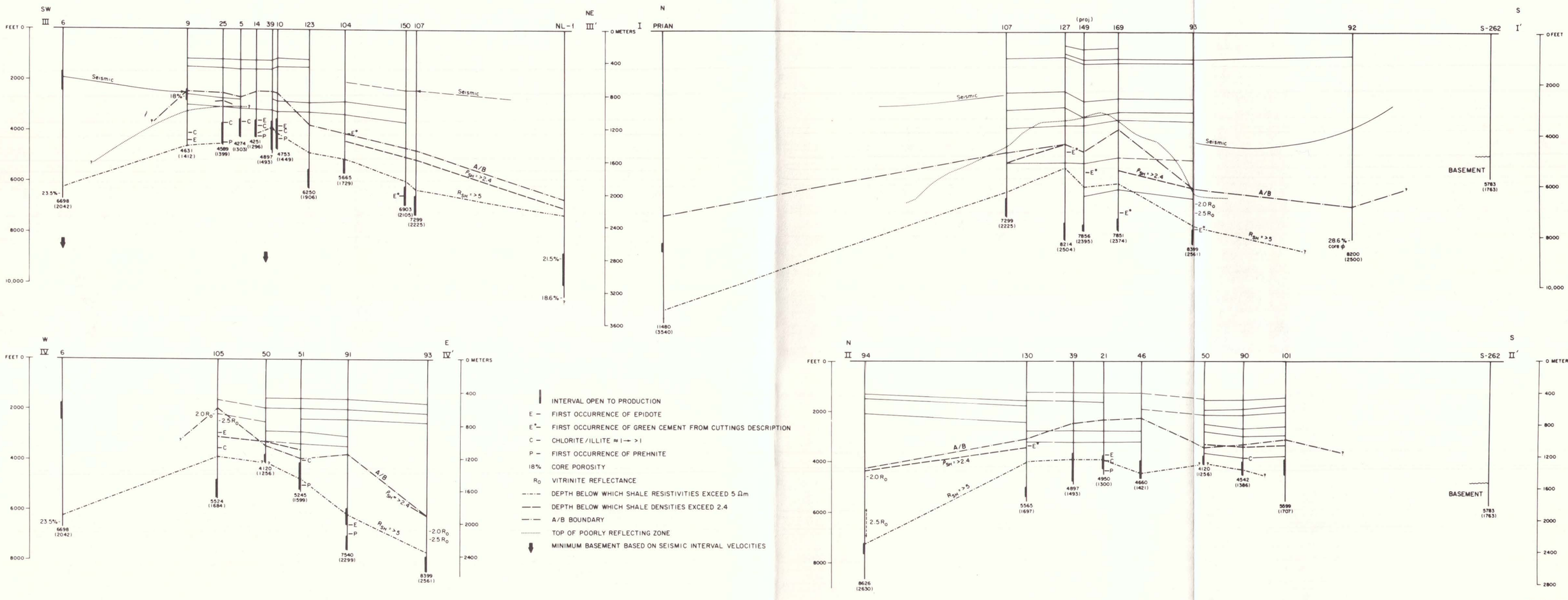


Figure 21. Geometric relationship between sedimentary strata and the hydrothermal alteration zone and correlation of various alteration horizons on cross-sections I-I′, II-II′, III-III′, and IV-IV′.

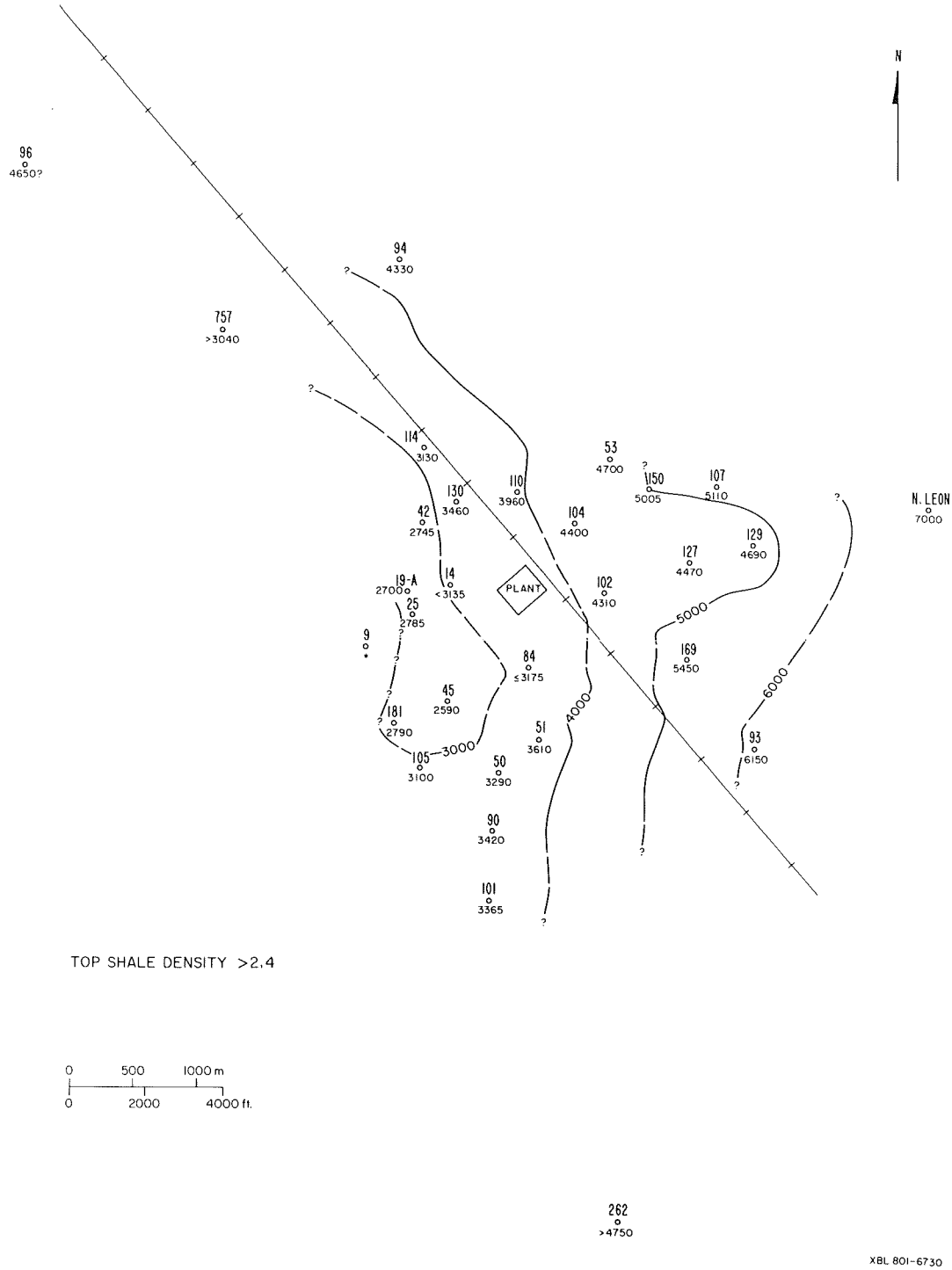


Figure 22. Map of the depth below which shale densities exceed 2.4 (top of high-density shales). Contours are in feet.

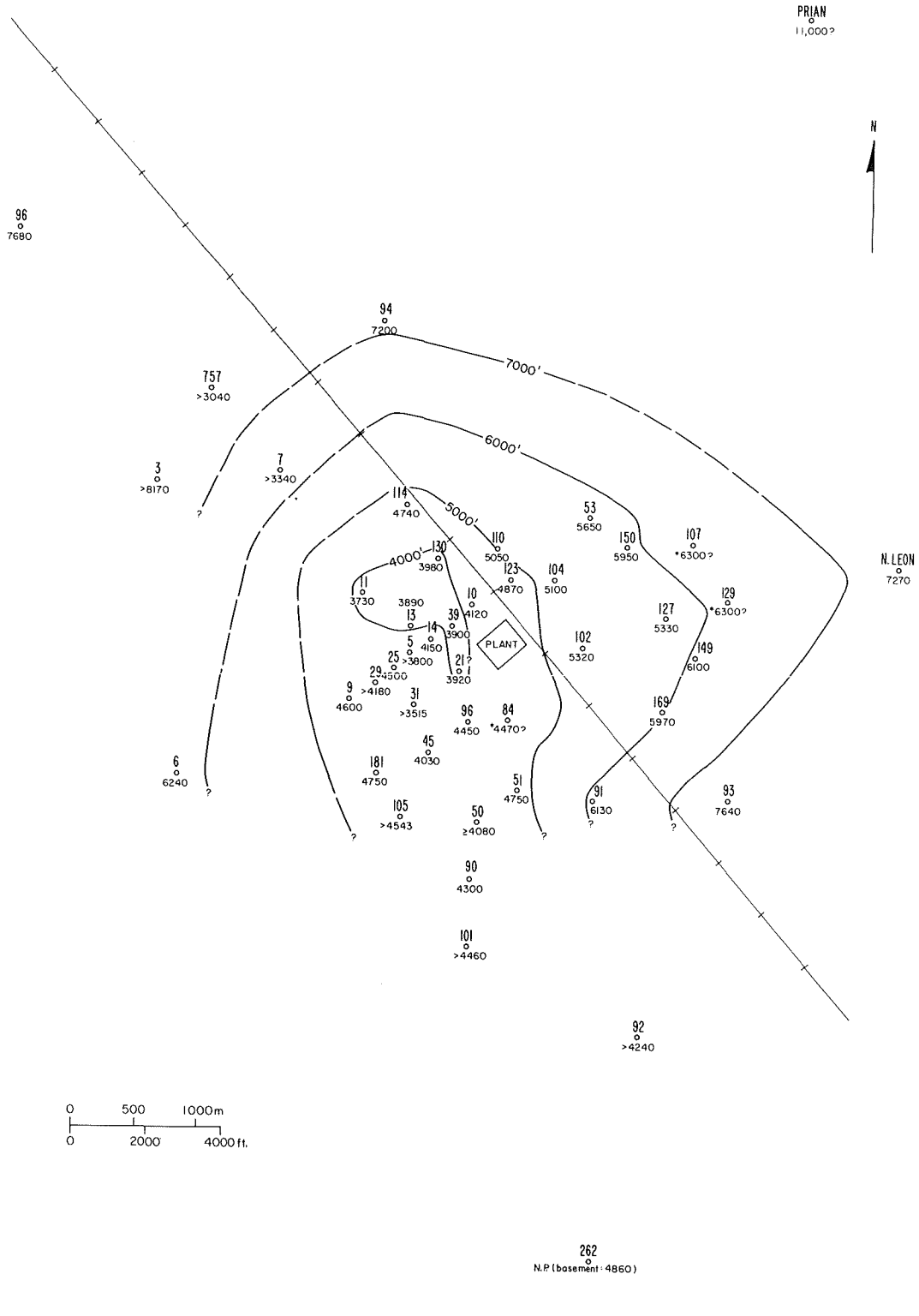


Figure 23. Map of the depth below which shale resistivities exceed 5 ohm-m (top of high-resistivity shales). Contours are in feet.

## Hydrothermal Minerals

Elders et al. (1978, 1979) have determined the distribution of hydrothermal minerals in sandstones and shales in 23 wells at Cerro Prieto by x-ray diffraction analysis of well cuttings. They found a dome-like pattern of hydrothermal mineral horizons similar to the isotherm pattern from borehole temperature surveys, which led them to conclude that temperature is the principal control over the observed mineralization (Figure 24). The shallowest hydrothermal mineralization occurs in the older producing area. Three mineral horizons were selected from the data in Elders et al. (1978) and plotted on the cross sections in Figure 21. The horizons consist of the first occurence of epidote, ~~in which~~ the chlorite/illite ratio increases to greater than 1, and the first occurrence of prehnite. In addition, the first occurrence of green cement (probably epidote), based on cuttings descriptions by CFE personnel, is also shown.

Not surprisingly, the configuration of the hydrothermal mineral horizons conforms in general to the dome-like pattern of the consolidation, density, and resistivity transitions, which suggests that these changes in physical properties of the sediments were caused by hydrothermal alteration. Maps of the depths to various mineral horizons in Elders et al. (1978) are similar to the shale density and resistivity horizon maps in Figures 22 and 23. The discordant geometry of the altered zone with respect to the strata indicates a localized heat source rather than burial diagenesis (burial metamorphism).

## Subsurface Temperatures

The depths corresponding to a borehole temperature of 250°C are also given on the cross sections in Figure 21. This temperature was arbitrarily selected to represent the configuration of the high-temperature zone in the

NOT GIVEN ON FIGURE! (DRAFTING ERROR)

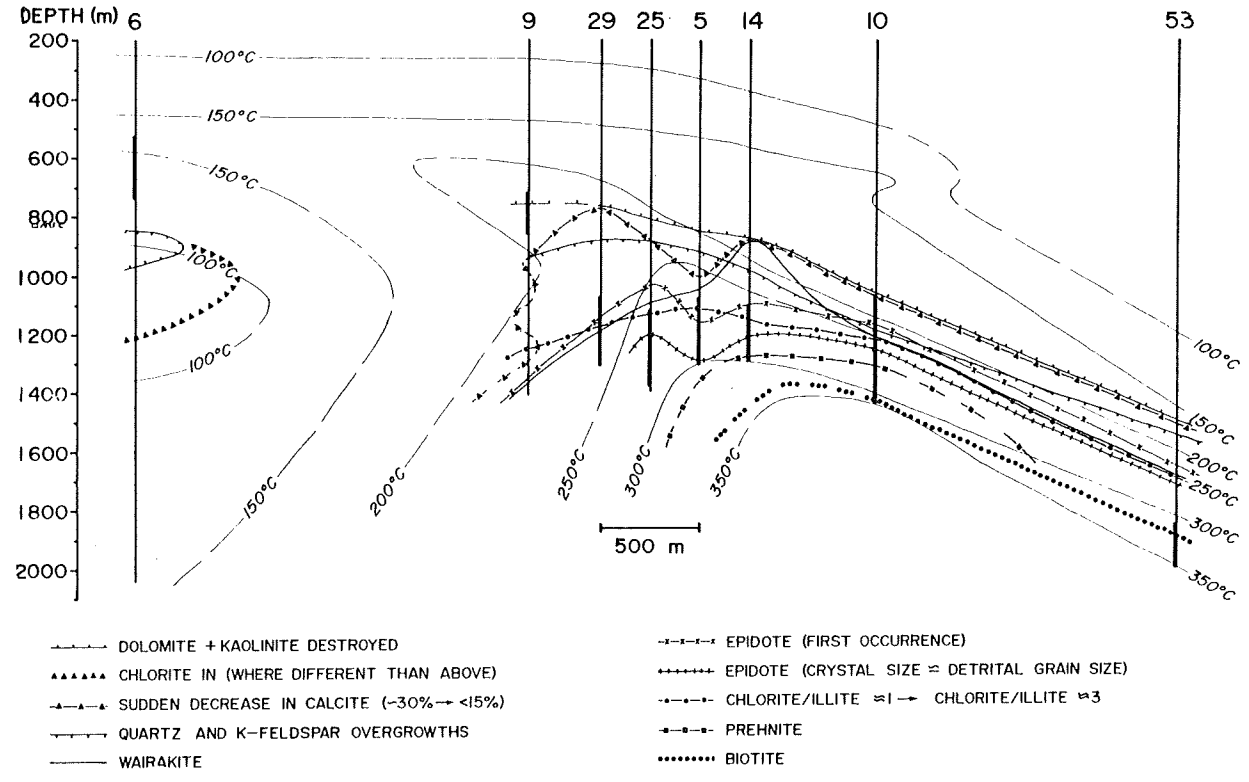


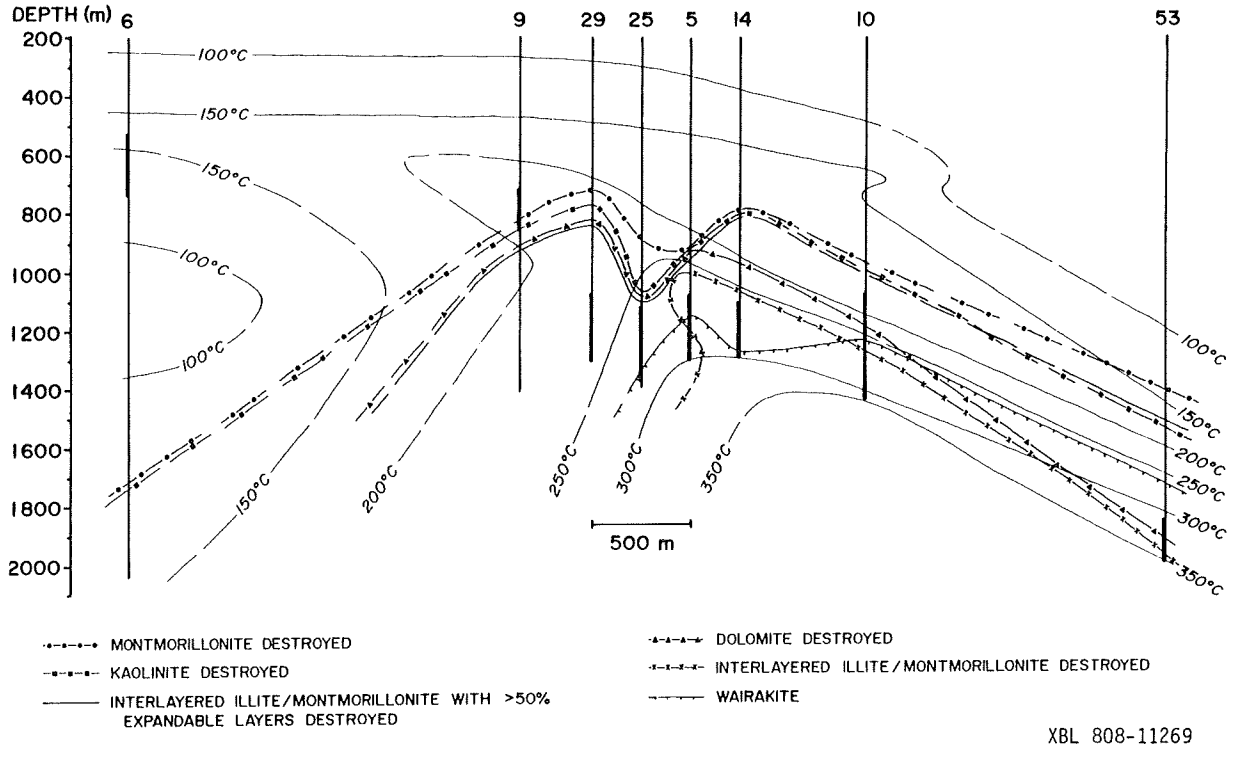


Figure 24. Correlation of hydrothermal mineral horizons and borehole temperature isotherms (Elders et al., 1979).

field area. Since temperature survey data for many of the wells were not available to this study, it was not possible to draw a 250°C isotherm across the cross sections.

It must be emphasized that temperatures measured in the borehole are commonly lower than the true formation temperature because of cooling by drilling fluids in the borehole. Several temperature surveys were made in some wells. In such cases, the temperature-depth curves generally exhibit a systematic shift to higher temperatures with increasing time since the last circulation. The depths to 250°C were taken from the curve with the longest lapsed time, which varies from well to well. For wells M-93 and M-105, temperature surveys during steam discharge were available (Barker, 1979), and these were helpful in estimating the actual formation temperature. For the other wells for which the 250°C depth is given in the cross sections, however, the hottest temperature surveys may still be too cool in some cases. Consequently, the 250°C depth should be regarded only as a maximum depth, i.e., the 250°C formation temperature may actually occur at shallower depths than indicated on the cross sections.

Although the borehole temperature data indicate that the consolidated, high-density, high-resistivity shales correspond to high-temperature conditions, the 250°C depth in Figure 21 is quite variable in detail with respect to the consolidation, density, and resistivity transitions described above. In addition to the borehole cooling problem, these deviations may reflect cooling of the subsurface since the thermal "event" that caused the hydrothermal alteration of the sediments below the A/B boundary. Other evidence of post-alteration cooling will be discussed later.

Barker (1979) determined vitrinite reflectance-depth trends for four

Cerro Prieto wells (M-84, M-93, M-94, and M-105). Because this physical property is a measure of maximum temperature conditions, isoreflectance levels would be expected to conform more closely to the physical and mineralogical alteration horizons than borehole temperature isotherms. There is an abrupt increase in vitrinite reflectance at the A/B boundary from less than 1.0 above to greater than 3.0 a few hundred meters below. Correlation of vitrinite reflectance with burial diagenesis and metamorphism in other areas indicates burial diagenesis down to the A/B boundary and metamorphism below (Lyons, 1979). From Barker's reflectance-depth trends, the depths to 2.0 and 2.5 $R_o$ were plotted on the cross sections. These reflectance values consistently are between the A/B boundary and the top of the high-resistivity shales. Thus, as anticipated, this paleotemperature indicator is more conformable to the alteration horizons than to borehole temperatures.

Productive Intervals

With the exception of the relatively cool, shallow production on the northwest flank of the field, the geothermal production intervals generally straddle or underlie the top of the high-resistivity, high-density shales. This suggests that the geothermal resource is related to the same heat source responsible for the hydrothermal alteration of the sediments. The thermal history of this area will be discussed later.

## 6. NATURE OF THE GEOTHERMAL RESERVOIR

Because of the evidence of induration and metamorphism below the A/B boundary, previous workers concluded that interstitial or matrix porosity and permeability is poorly developed in the deeper part of the Cerro Prieto

field. Observations of fractures in cores suggested fractured reservoirs. This conclusion is supported by correlations of sandstone porosity/permeability with burial diagenesis and metamorphism in a variety of sedimentary basins (e.g., van de Kamp, 1976; Lyons, 1978, 1979). However, evidence will be presented below that secondary matrix porosity and permeability are well developed below the A/B boundary throughout the Cerro Prieto field.

Well Log Evidence

Resistivity, density, and sonic logs in the altered zone indicate that whereas the shales are indeed low-porosity, highly indurated rocks, the sandstones commonly have fair to good porosities (15% to 35% or higher). The porosity calibration of the density log response by Schlumberger is based on quartz-rich sandstones, which is consistent with the sandstone composition data discussed earlier. These relatively high log porosities were corroborated by core porosity measurements by CORELAB, Inc. (18% to 28.6% below the A/B boundary) which are given on the cross sections.

An example of the resistivity and density log patterns above and below the A/B boundary is shown in Figure 25. Sand resistivities are higher than shale resistivities above the A/B boundary, but below the top of the high-resistivity shales, most of the sandstone intervals have lower resistivities. Shale densities are normally higher both above and below the A/B boundary, but the density difference between sandstones and shales below A/B is generally much greater than the density difference between sands and shales above A/B. As illustrated in the density-depth plots in Figure 26, while the shales exhibit the expected marked increase in density at the top of the altered zone, most of the sandstone intervals show a much smaller change in density (porosity). Some sandstone porosities in the altered zone are

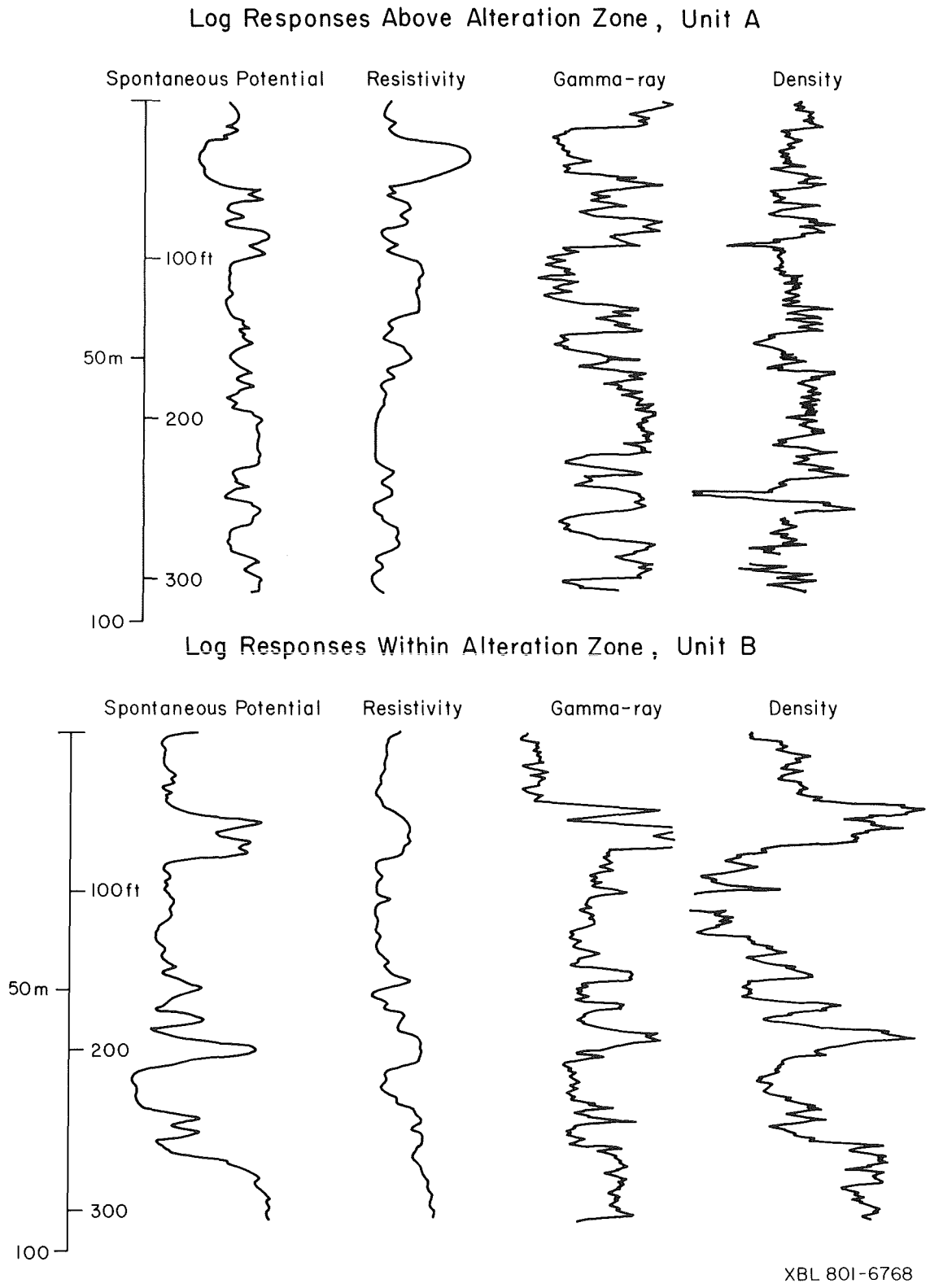


Figure 25. Typical example of the contrasting resistivity and density log response patterns for sands and shales above and within the altered zone. The lower density curve was shifted to the left (lower density) with respect to the upper density curve for display purposes.

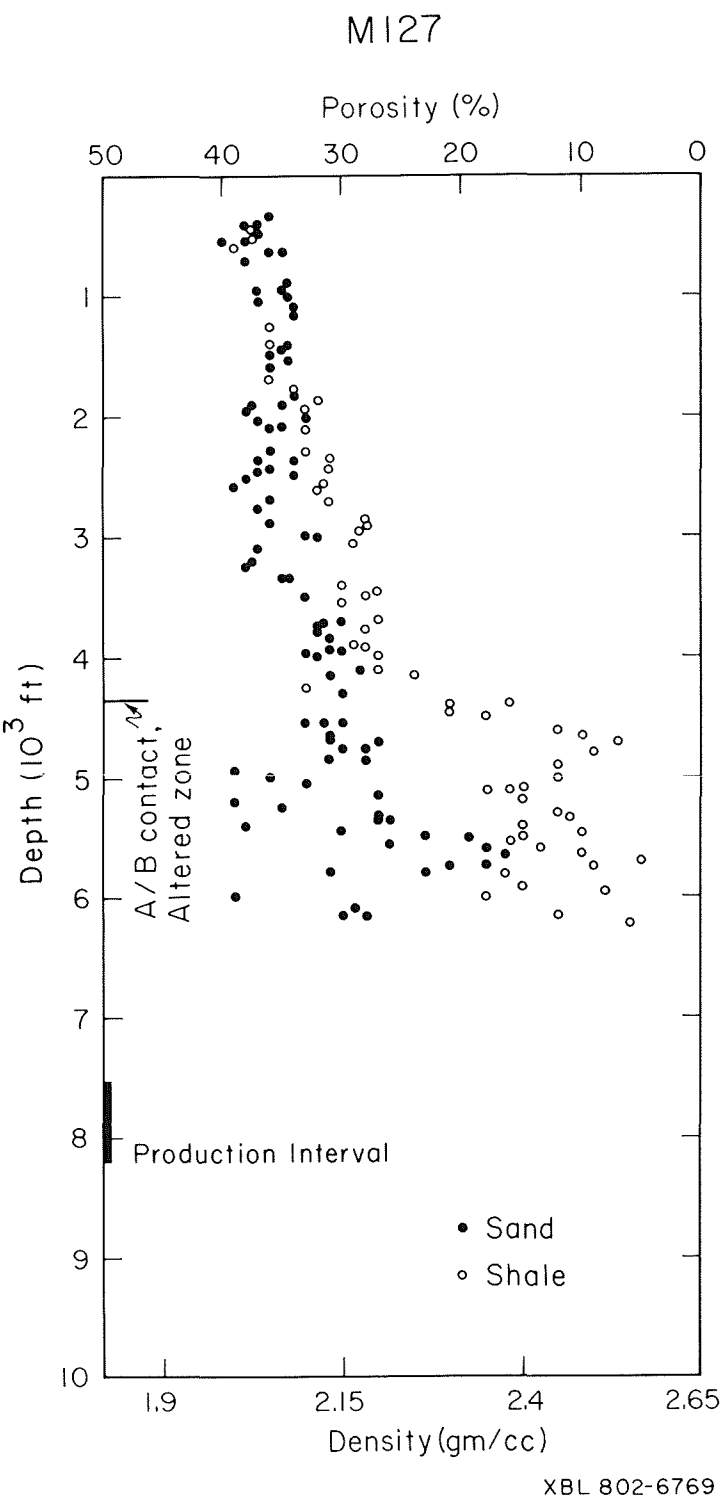


Figure 26. Examples of density-depth plots illustrating the marked increase in shale densities at the top of the altered zone, but much smaller change in density in sandstones.

apparently even higher than those above the A/B boundary. The occurrence of fair to good sandstone porosity interbedded with low-porosity, metamorphosed shales implies secondary porosity development by solution of chemically unstable framework grains and pore-filling material. Typically, there is more scatter in the density-depth relationship for sandstones below A/B than for sands above A/B which suggests variation in the degree of secondary porosity development.

In contrast, in the M-96 well, which is a nonproductive well northwest of the field, the density-depth trend suggests progressive porosity destruction with increasing burial depth (Figure 27). The A/B boundary was not picked in this well by CFE, but below the 2.4 shale density horizon, sandstone porosities decrease systematically from about 19% to 6%. The borehole temperature surveys indicate that M-96 is presently cool, but the sandstone density-depth trend for M-96 exhibits higher densities (lower porosities) versus depth than the trend for M-94, which is a much hotter well. This suggests that the porosity destruction in M-96 is related to higher paleotemperature conditions. Secondary solution porosity is apparently not very significant in M-96. Differences in the alteration history between the producing area and this well will be discussed later.

Petrographic Evidence

To check the secondary solution porosity idea, alterations and textural relationships were examined in the petrographic study referred to in Section 3 (Depositional Model; see Table 1). All samples are from the indurated zone (below the A/B boundary). The rocks were impregnated with blue epoxy resin before cutting the thin sections. The blue resin fills the pore space and facilitates the recognition of porosity.

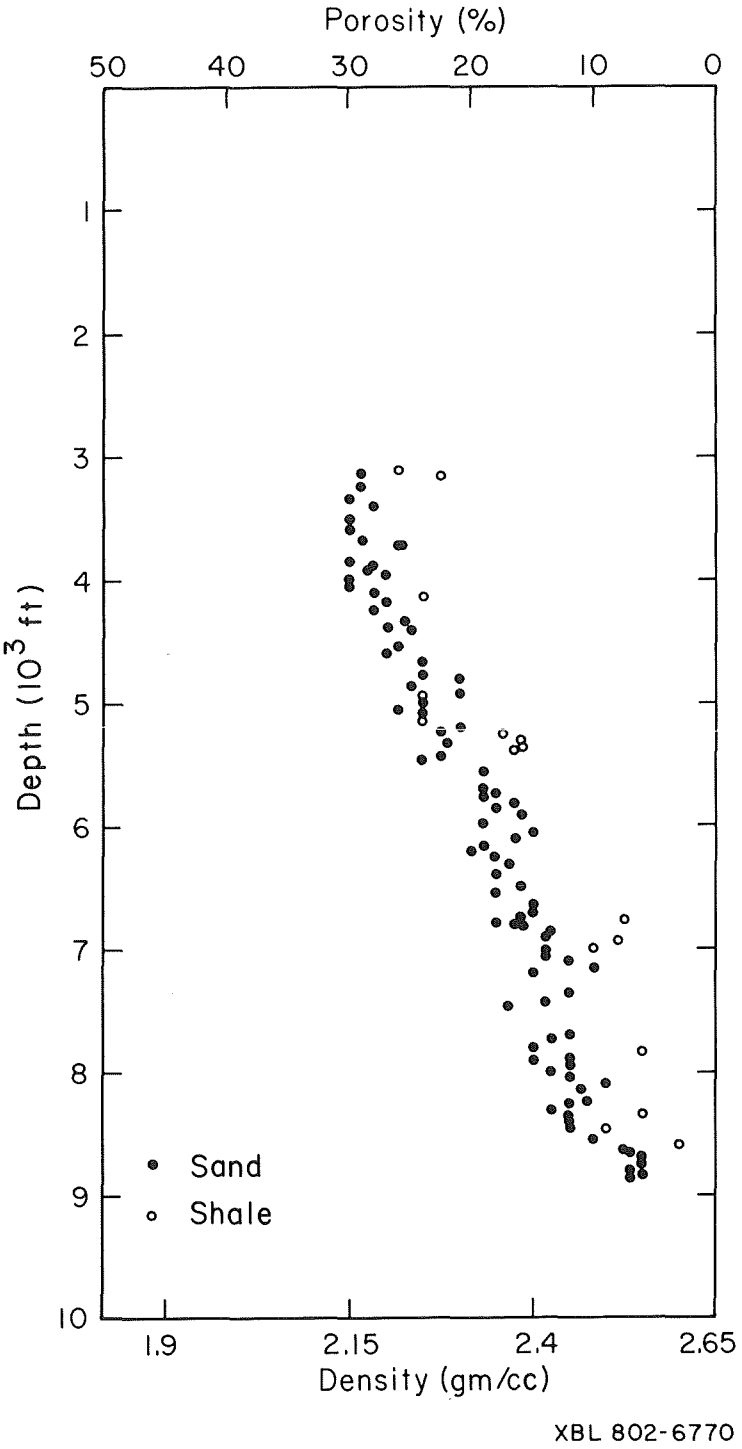


Figure 27. Density-depth trend in the M-96 well illustrating progressive porosity destruction with depth and the apparent absence of significant secondary solution porosity.

The sandstones are very fine- to coarse-grained and are moderately to well sorted. Matrix clays are 1% or less in most samples. Alterations similar to those previously described in Elders et al. (1978, 1979) are common. The most abundant cement in these sandstones is pore-filling carbonate. Quartz grain-overgrowth cement and epidote pore-filling cement are minor constituents.

Textural relationships suggest that cementation reduced sandstone porosities to less than 10% below the A/B boundary. However, subsequent solution of chemically unstable framework grains (mainly feldspar and some volcanic fragments) and carbonate cement resulted in increased porosity to 28% or more. These relationships are illustrated in Figures 28 to 31. In the presently cool M-96 well, solution porosity is not as well developed as in the producing wells.

The texture typically varies from tightly cemented to apparently isolated "vuggy" porosity to interconnected porosity in the same thin section, which suggests that permeability will vary from poor to good in these porous hydrothermally altered sandstones. The core permeability measurements support this suggestion. The variability in sandstone permeability in the altered zone is illustrated by the core porosity-permeability crossplot in Figure 32.

Fracture Versus Matrix Permeability

Thus the density logs, core measurements, and thin sections consistently indicate fair to good sandstone porosities in the hydrothermally altered zone. The textural relationships clearly support the above interpretation that these anomalously high porosities are due to post-alteration solution. It follows then that matrix porosity and permeability are significant even in

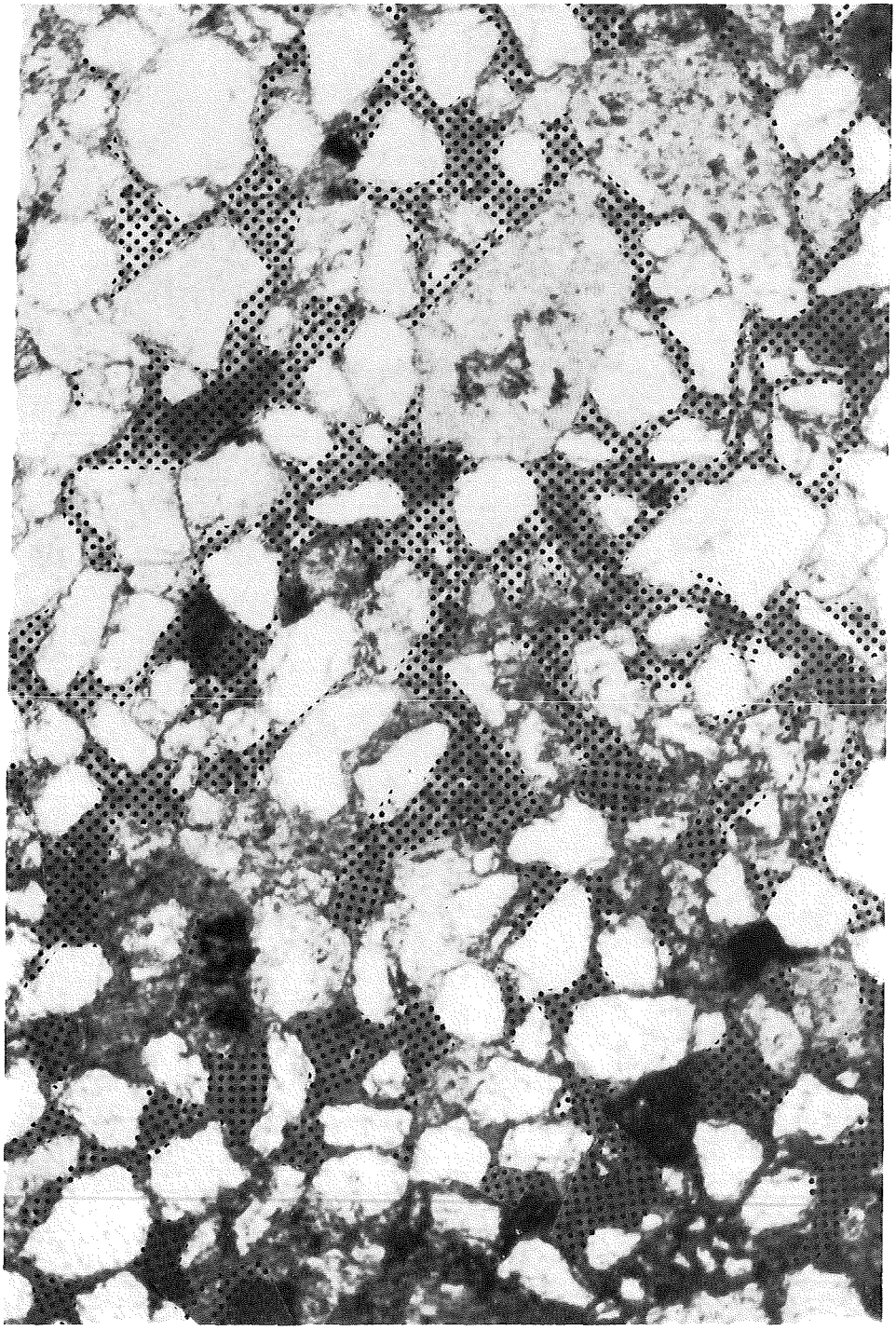

CBB 802-2543

Figure 28. Photomicrograph of sandstone core sample from well M-20, at 915.3 m depth, plane polarized light. The dotted areas in this view are pores mostly resulting from removal of carbonate cement and feldspar. Elsewhere in this section, the cement is present. Measured porosity is 23.7% in this rock. View is 1.2 mm across.

CBB 802-2541

Figure 29. Photomicrograph of sandstone at 915.3 m depth in well M-20 showing porosity in dot pattern. On the right side of the view an area cemented by carbonate is present. The packing arrangement of detrital grains is similar in both cemented and cement-free areas. View is 1.2 mm across.

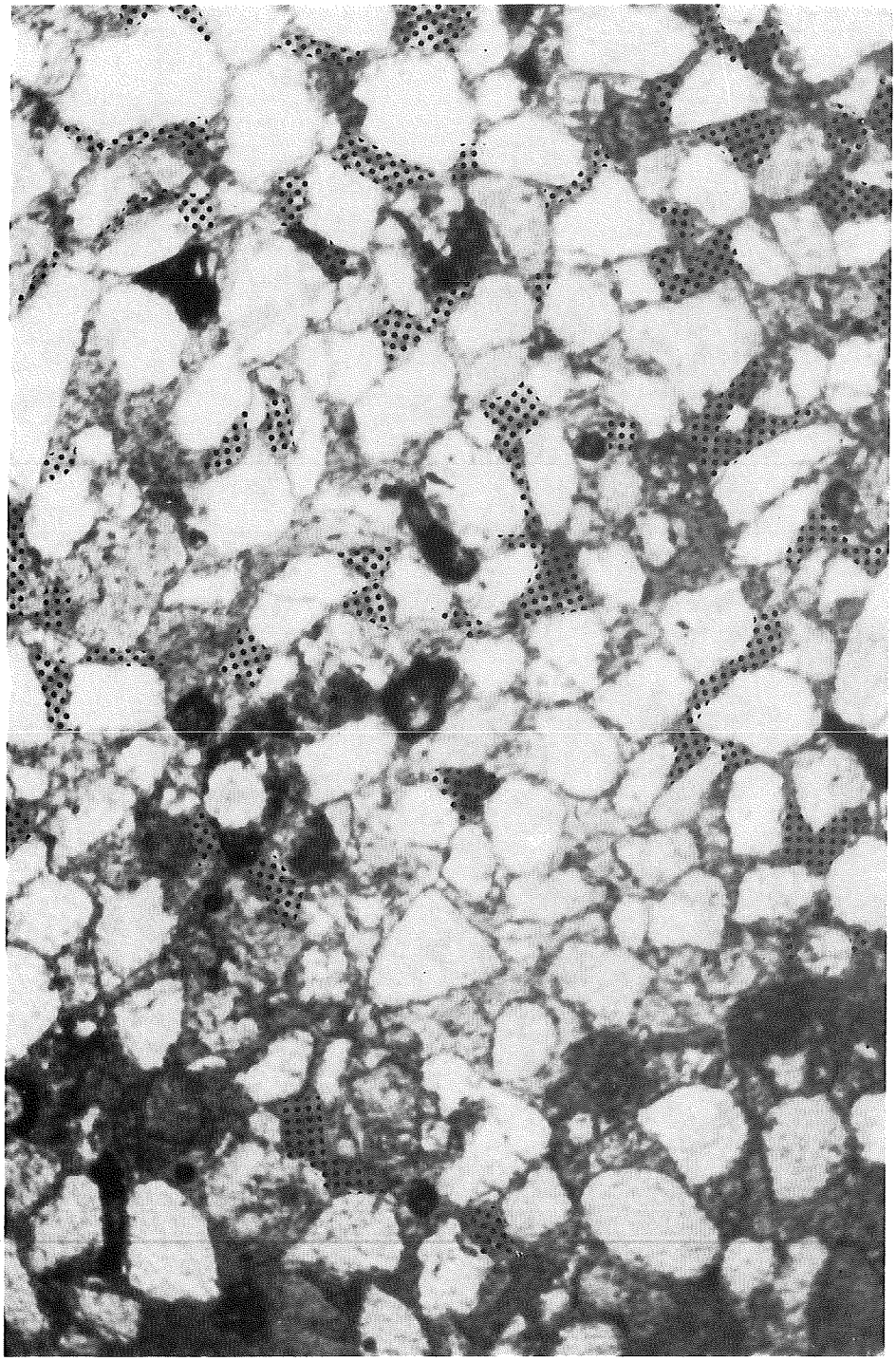

CBB 802-2547

Figure 30. Sandstone in well M-96 composed of angular to well-rounded grains. Dotted areas are pores. In the left center of the view is a feldspar grain with four holes resulting from partial leaching of the grain. This sample is from 1981 m depth. View is 1.2 mm across.

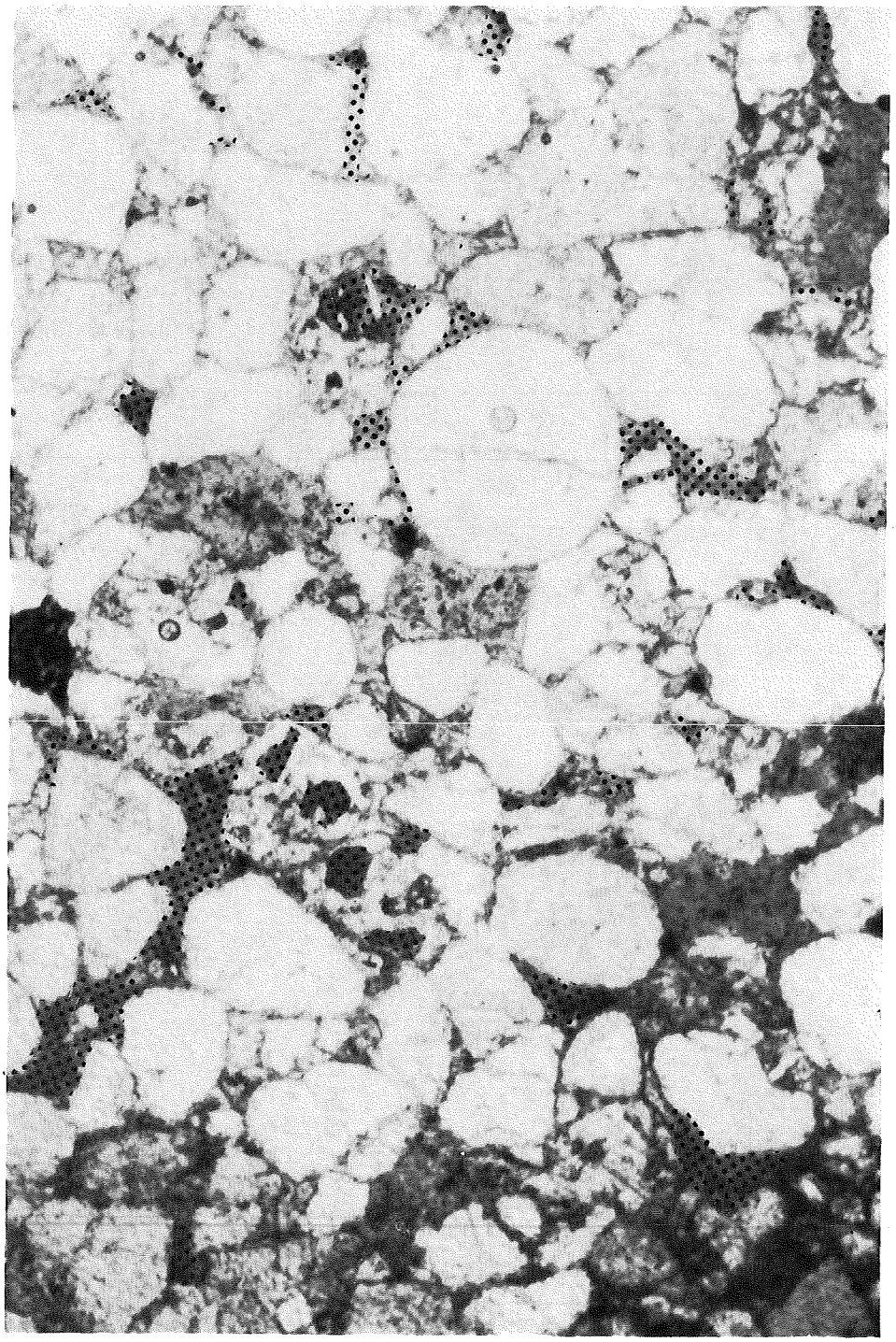

CBB 802-2545

Figure 31. Sandstone, well M-96 at 1979 m depth. This is a fine grained, moderate to well sorted rock, with secondary porosity shown in a dot pattern. The grain in the center is a partly leached feldspar. View is 0.5 mm across.

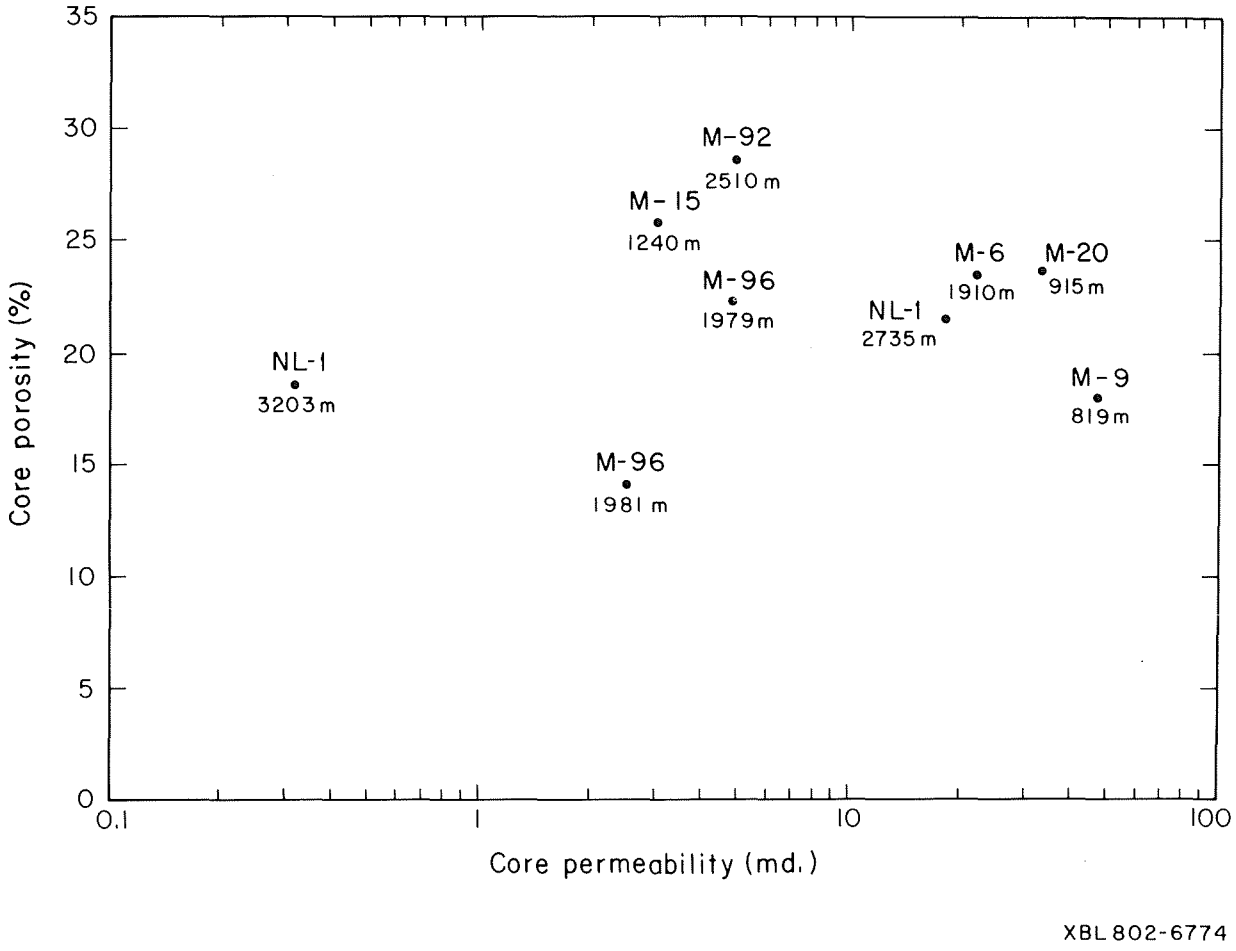


Figure 32. Core porosity versus permeability for sample from the altered zone (measurements by CORELAB, Inc.).

the deeper reservoirs.

Descriptions of cores from 12 wells supplied by CFE suggest that open fractures (fracture permeability) are unusual in the hydrothermally altered zone. Fracture permeability may be significant near faults, although the core descriptions suggest that this is generally not the case. Fractures were observed in both sandstones and mudstones.

Some fractures are filled with sediment, mainly fractures in mudstone filled with sandstone, indicating injection of unconsolidated sediment into adjacent, more consolidated fractured sediment. Such fracturing apparently occurred before hydrothermal alteration.

Post-induration fractures are commonly sealed by hydrothermal mineralization as described by Elders et al. (1978, p. 76). They interpreted repeated fracturing and sealing in the altered zone based on "multiple and cross-cutting mineral veins." Calcite was mentioned as a common vein mineral as fracture filling. Some of the calcite may represent reprecipitation of the calcite cement removed from the sandstones. Perhaps some of the other vein minerals may be related to the solution of unstable grains in the sandstones (i.e., feldspars and volcanic fragments).

Although fractures may be an important contributor to reservoir permeability locally, secondary matrix porosity and permeability appear to be more important volumetrically in the reservoirs of the Cerro Prieto field.

## 7. SURFACE GEOPHYSICAL DETECTION OF GEOTHERMAL ANOMALY

### Resistivity

Generally speaking, hydrothermal alteration of sediments results in the formation of authigenic cements in sandstones and clay mineral transformations

in shales, both of which causes a decrease in primary porosity and an increase in resistivity. This effect may be offset to some degree by the development of secondary solution porosity in sandstones as discussed in the previous section. Another offsetting factor is the increase in pore fluid salinity related to hydrothermal reactions which produce higher concentrations of ions in the pore fluid. The effect of the salinity change depends on the net porosity loss in the altered zone. In an area where lateral and/or vertical gradations from nonmarine to marine depositional conditions occurred, the resulting salinity variations would complicate the resistivity response and obscure, to some degree, the effects of hydrothermal activity.

The interpreted surface resistivity along seismic line D-D′ by Wilt et al. (1979) shows a high-resistivity body below 800 m, which approximately coincides with the productive zone in the older part of the field. The researchers relate this body to porosity loss by hydrothermal alteration because it correlates well with the altered zone (cross section III-III′ in Figure 21). The top of the high-resistivity shales observed on the well logs (Figure 21) shows good agreement with the high-resistivity body interpreted from the surface survey.

Wilt et al. (1979) also recognized a similar high-resistivity body on their profile D-D′ northwest of the field in an area which is presently cool. This body correlates with a high-gravity "ridge" that wells Q-757 and M-96 reveal is due to densified sediments (see Section 4, Structure).

In general, detecting geothermal anomalies in this region on the basis of surface resistivity data alone could be difficult and risky for the reasons discussed above. Moreover, resistivity surveys without proper,

detailed interpretation might very well supply misleading information.

Magnetics

According to Fonseca L. and Razo M. (1979, p. 36), "Hydrothermal reactions and metamorphism also seem to affect magnetic anomalies." This is not apparent, however, in the ground magnetic data obtained by CFE (Figure 20). The x-ray diffraction analyses of well samples reported by Elders et al. (1978) indicate that the only magnetic mineral present in the altered zone is the weakly magnetic sulphide pyrrhotite, which is generally absent. Where detected, the concentrations were generally less than 1% by weight. Therefore, magnetics does not seem to be a very promising detection method for the Cerro Prieto region.

Gravity

As mentioned earlier in the Structure section, positive gravity anomalies are associated with most geothermal anomalies in the Imperial Valley due to densification (porosity loss) of the sediments by hydrothermal alteration. Coincident positive gravity and magnetic anomalies suggest basement highs, which may or may not be associated with hydrothermal activity, but a positive gravity anomaly coincident with a negative magnetic anomaly, or absence of a magnetic anomaly, suggests densified sediments above basement.

At the Cerro Prieto field, hydrothermal alteration also produced densification, but as discussed in the preceding section, later removal of unstable grains and cement from the sandstones by solution resulted in anomalously low density sandstones interbedded with high-density shales. Consequently, the effect of the densification on gravity depends on the percentages of sandstone and shale which varies laterally as shown on the stratigraphic cross sections in Figures 4-7. Not surprisingly, there is

no positive gravity anomaly coincident with the production area (Figure 13).

It is not yet clear whether low-porosity, high-density altered rocks (as in the Imperial Valley and perhaps northwest of the field) or higher porosity, lower density altered rocks showing secondary solution porosity (as at Cerro Prieto) are more typical in other geothermal anomalies in the Mexicali Valley area.

Reflection Seismic Profile

The A/B boundary or top of the hydrothermal alteration zone does not appear as a reflection on the seismic profiles for several reasons. First, the top of the altered zone is a transition in the degree of consolidation or induration, not an abrupt change, which means a long-wavelength, low-frequency change in acoustic impedance. Frequencies less than 10 Hz would be required to produce a reflection from this transition. In the Cerro Prieto seismic data, however, frequencies less than 16 Hz were eliminated by the bandpass filter applied in the data processing. Second, even if very low frequencies had been recorded and preserved in the seismic data, higher-frequency primary reflections and noise would obscure the discordant low-frequency reflection. Third, well-log data indicate that the magnitude of the acoustic impedance change at the top of the altered zone varies considerably across the field area due to two factors. The variation of magnitude is caused by change in the burial depth of the overlying sediments and change in the percentage of relatively low acoustic impedance sandstones due to secondary solution porosity in the altered zone. Where such sandstones predominate over densified shales in the upper part of the altered zone, there may actually be a polarity reversal in the acoustic impedance change. These lateral variations in the magnitude and polarity of the acoustic impedance change would also make it very difficult to recognize

a coherent reflection corresponding to the top of the altered zone. Finally, although well correlations suggest a rather simple dome-like configuration for the top of the altered zone, the detailed geometry may be much more irregular, which would also complicate the recognition of a reflection from this acoustic impedence transition.

A reflection-poor zone, cross-cutting several strata and coincident with the hydrothermally altered zone, was observed at the East Mesa geothermal field in the Imperial Valley by van de Kamp (in Howard et al., 1978). This zone is characterized by relatively low matrix porosities and permeabilities and by higher velocities and densities than in the laterally equivalent lower temperature strata. The dome-like configuration of the reflection-poor zone agrees well with a gravity maximum over the field. The productive intervals in the East Mesa field are within or just above this zone.

A similar reflection-poor zone was observed at Cerro Prieto on seismic profiles A-A′(Figure 12), B-B′, and D-D′ (Figure 11). Although there is not sufficient seismic reflection data coverage to map this dome-like zone as at East Mesa, it agrees reasonably well with the producing area on these profiles. With the exception of the shallow production on the northwest flank of the field, most of the producing intervals are within the reflection-poor zone. A comparison of the top of this zone and the induration, density resistivity, hydrothermal mineral, temperature, and vitrinite reflectance horizons discussed in the Hydrothermal Alteration section can be seen on cross sections I-I′ and III-III′ in Figure 21.

NOT ON FIGURE

It was suggested that the lack of reflections at East Mesa may be due to extensive fracturing of the relatively brittle rocks in the high-temperature zone resulting in dispersion of seismic energy. However,

it was pointed out (Section 6, Nature of the Geothermal Reservoir) that open fractures may be relatively uncommon in the hydrothermally altered zone at Cerro Prieto. Perhaps closely spaced older faults contributed significantly to the development of this reflection pattern in the older producing area by disrupting reflection continuity. A more significant factor at Cerro Prieto, however, may have been the obliteration of acoustic impedance layering (strata) by porosity destruction due to hydrothermal alteration. Even though later preferential solution of unstable components in sandstones produced fair-to-good secondary porosity, the original acoustic impedance layering probably was not "recreated" because of the vertical and lateral variability of the solution porosity.

Therefore, in either the East Mesa situation (porosity destruction and fracturing) or the Cerro Prieto situation (porosity destruction followed by porosity enhancement), the seismic reflection method could be a good approach for identifying geothermal targets. Great caution is necessary, however, because structural complexities, dominantly one-lithology sequences, and shallow basement highs may produce similar seismic reflection patterns. By utilizing other geophysical data, at least some of the alternatives may often be eliminated. Moreover, since adequate seismic reflection coverage for geothermal exploration may be prohibitively expensive, this geophysical method is probably most useful for delineating the limits of the geothermal resource after a discovery has been made.

## 8. THERMAL-TECTONIC HISTORY

The induration or densification of the sediments below the A/B boundary by hydrothermal alteration preceded the development of secondary solution

porosity in the sandstones and the repeated fracturing and sealing of fractures recorded by mineral veins. This suggests a relatively long period of hydrothermal activity in the Cerro Prieto area.

The culmination of the A/B boundary (at the top of the main altered zone) in Figure 21, in the older producing area (wells M-5,M-9,M-10,M-14,M-25 and M-39 on cross section III-III′) is nearly flat. This implies that the top of the hydrothermal zone was near the surface, i.e., the stratigraphic horizon just above the flat culmination of the altered zone approximately dates the densification of the sediments.

The well log correlations in this study revealed localized angular unconformities in the field area that were related to older fault displacements. (This occurs between wells M-127 and M-149 on cross-section I-I", M-50 and M-90 on cross-section II-II′, M-10 and M-39 on cross-section III-III′, and M-51 and M-91 on cross-section IV-IV′. See Figures 4-7 or Figure 21). The stratigraphic position of many of these unconformities appears to be very close to the upper limit of the altered zones. This suggests a relation between the northeast-southwest and north-northeast to south-southwest faulting and the hydrothermal activity which caused the densification of the sediments.

A local angular unconformity between M-6 and M-9 is indicated by discordant reflection geometry on seismic profile D-D′ (Figure 11). This discontinuity seems to be at about the same stratigraphic horizon as the culmination of the altered zone and many of the unconformities recognized in the main producing area. It is interesting to note that the shallow production zone west and northwest of the main production (M-3, M-6, M-7, M-9, M-11, M-29, and Q-757) appears to straddle this unconformity horizon. It represents

an offshoot of the main hydrothermal zone (refer to the isotherm configuration in Figure 24). This is somewhat analogous to the intrusion of an igneous sill from a stock into surrounding sediments.

According to de Boer (1979), paleomagnetic data indicate that eruptions of the Cerro Prieto volcano began approximately 110,000 years ago. The unconformities discussed above were followed by the deposition of about 2500 to 3500 ft (762 to 1067 m) of sediments. Although the unconformities and the older faulting cannot be related to the initiation of volcanism directly, the depositional rates suggest that deposition of the post-unconformity sediments in the past 110,000 years is certainly reasonable. This is supported by the interpreted thickness of the Holocene in the Colorado River delta plain southeast of Cerro Prieto (van de Kamp 1980, oral commun.) and by the calculated depositional rates for the New River delta at the south end of the Salton Sea (Stephen and Gorsline, 1975).

Therefore, it appears that the onset of the northeast-southwest and north-northeast to south-southwest faulting, the onset of hydrothermal activity, and the onset of the Quaternary volcanism were roughly synchronous. The topographic elongation of the Cerro Prieto volcano indicates northeast-southwest structural control. It seems reasonable that the rise of isotherms in the field area and the upward movement of rhyodacitic magma to the northwest was in response to the extensional faulting. The age of this major thermal-tectonic event is not clear, but the date of the oldest known eruption at the Cerro Prieto volcano could be considered a minimum age.

Episodic thermal and tectonic activity from the event described above to the present is indicated by the paleomagnetic evidence of at least five major eruptive phases of the Cerro Prieto volcano (de Boer, 1979); the evidence

of repeated fracturing and sealing of fractures by hydrothermal mineralization (Elders et al., 1978); and the present thermal springs and seismicity. The secondary solution porosity in the altered sandstones developed during this period. It seems likely that low-salinity waters moved laterally into the altered zone from the cooler unaltered sediments. As these waters heated up, increasing their chemical activity, solution of the unstable components in the sandstones began. It is not known where all the dissolved material was precipitated, but the mineralization of fractures may acount for at least part of it. This process was probably more effective at times when open faults and fractures were present in the altered zone. Secondary porosity may have developed at different times throughout the field area according to the availability of open faults and fractures or gradually in response to the repeated fracturing indicated by the mineral vein relationships.

As discussed in Section 6, that secondary solution porosity is not very significant in M-96, which is a cool well northwest of the field. High densities and resistivities in the lower part of the well, as well as an indurated texture observed in thin sections, suggest cooling since the main thermal-tectonic event. Secondary solution porosity development may have been limited by the relatively low subsurface temperatures following the induration of the sediments.

It was mentioned in Section 5 (Hydrothermal Alteration) that, in detail, the 250°C isotherm does not parallel the consolidation, density, and resistivity transitions. These deviations may also suggest localized cooling since the main thermal-tectonic event.

The history of the Cerro Prieto area from the formation of the basin to the present is summarized in Table 2.

TABLE 2. GEOLOGIC HISTORY OF THE CERRO PRIETO GEOTHERMAL FIELD: HISTORY OF THE AREA FROM FORMATION OF THE BASIN TO THE PRESENT

| | | |
|---|---|---|
| I. | Basin formation | Miocene |
| II. | Early stage basin fill including volcanics | Miocene |
| III. | Onset of Colorado delta progradation filling trough from northeast | Mid-Pliocene |
| IV. | Termination of lithofacies I deposition west of field and shoaling of marine connection to Imperial Valley area | Middle Pleistocene |
| V. | Onset of NE-SW and NNE-SSW faulting. Onset of thermal activity: (a) volcanism northwest of field, and (b) induration of sediments by hydrothermal alteration | Late Pleistocene (110,000 years or older) |
| VI. | Episodic faulting and thermal activity: (a) repeated faulting, fracturing, and fracture mineralization, (b) secondary solution porosity, (c) volcanism | Late Pleistocene to present |

# 9. CONCLUSIONS

1. The subsurface stratigraphy at Cerro Prieto is characterized by complex vertical and lateral variations in lithofacies, which is typical of deltaic deposits. The geothermal production zone is not a uniform reservoir layer overlain by a laterally continuous top-seal of low-permeability strata.

2. The deeper part of the stratigraphic section in the main producing area including the productive intervals, represents lower delta plain deposits of the ancestral Colorado delta. The arcuate lithofacies I belt (thick predominantly sand sequence) just west of the main producing area is interpreted as a deltaic coastal complex in a tide- or tide/wave-dominated delta. The area between the coastal-deltaic deposits and the basin margin alluvial fans on the flank of the Cucapa Range to the west was probably an area of at least intermittent marine deposition until the Middle Pleistocene.

3. In addition to the northeast-southwest and northwest-southeast fault trends, which have been emphasized in earlier fault interpretations of the Cerro Prieto area, north-south and north northeast-south southwest trends are also prominent. Older faults, reactivated older faults, and younger faults are present in the field.

4. Basement structure in the Cerro Prieto area is difficult to interpret because of very few basement penetrations by wells, anomalies within the basin fill (volcanics, dike/sill complexes, and densified sediments), and geophysical data coverage and data quality limitations. There does not seem to be any convincing geophysical evidence for a basement horst underlying the field as suggested by various workers in the past; instead there is apparently a general deepening of the basement in a southeasterly direction across the field.

5. The top of the well consolidated or indurated sediments has a dome-like configuration which cuts across the sedimentary strata. Shales in the indurated zone exhibit high densities and high resistivities on the well logs. The metamorphic mineral horizons, high temperatures, and high vitrinite reflectance at the top of the indurated zone indicate that the changes in the physical properties of the sediments were caused by hydrothermal alteration. Except for the relatively cool, shallow production on the northwest flank of the Cerro Prieto field, the geothermal production intervals generally straddle or underlie the top of the high-resistivity, high-density shales.

6. Sandstones in the hydrothermal alteration zone commonly have fair to good porosities (15% to 35% or higher) which resulted from the removal by solution of unstable grains and carbonate cement. Open fractures appear to be unusual in the altered zone based on core descriptions. While fractures may be an important contributor to reservoir permeability locally, secondary matrix porosity and permeability are considered to be more important volumetrically in the Cerro Prieto reservoirs.

7. Surface geophysical detection of geothermal anomalies in the Cerro Prieto region may be difficult from resistivity, magnetic, or gravity data. The occurrence of a reflection-poor zone coincident with the hydrothermal alteration zone at Cerro Prieto and at East Mesa suggests that the seismic reflection method may be a good approach, but other types of geophysical data are necessary to eliminate alternate sources of reflection-poor zones. This geophysical method would probably be most useful for field delineation because adequate seismic reflection coverage for geothermal exploration may be prohibitively expensive.

8. It appears that the older northeast-southwest and north northeast-south southwest faulting of the basin fill, the densification of the sediments below the A/B boundary by hydrothermal alteration, and the onset of Quaternary volcanism northwest of the Cerro Prieto field were roughly synchronous. The date of the oldest known eruption at the Cerro Prieto volcano (approximately 110,000 years B.P.) may be a minimum age for this major thermal-tectonic "event." Episodic thermal and tectonic activity occurred from this event to the present, including four major eruptive phases of the Cerro Prieto volcano, repeated fracturing of the densified sediments and sealing of the fractures by hydrothermal mineralization, and development of new faults and reactivation of older faults. The secondary solution porosity in the altered sandstones developed during this period. There may have been localized cooling in some areas since the "main" thermal-tectonic event.

## 10. ACKNOWLEDGMENTS

The authors gratefully acknowledge Lawrence Berkeley Laboratory of the University of California and the Comisión Federal de Electricidad de México for supplying the data used in this study. We also thank the personnel of both organizations for many beneficial discussions, including Maura O'Brien, Stephen Vonder Haar, and John Noble of Lawrence Berkeley Laboratory for reviewing the manuscript, Margot Harding for drafting the figures, and Cathy Donnelly for typing the manuscript.

This work was performed for the U.S. Department of Energy, Division of Geothermal Energy, under contract W-7405-ENG-48.

## 11. REFERENCES CITED


Abril G., A., and Noble, J. E., 1979, Geophysical well-log correlations along various sections of the Cerro Prieto geothermal field, in Proceedings, First Symposium on the Cerro Prieto Geothermal Field, Baja California, Mexico, September 20-22, 1978: Berkeley, Lawrence Berkeley Laboratory, LBL-7098, p. 41-48.

Albores L., A., et al., 1979, Seismicity studies in the region of the Cerro Prieto geothermal field, in Proceedings, First Symposium on the Cerro Prieto Geothermal Field, Baja California, Mexico, September 20-22, 1978: Berkeley, Lawrence Berkeley Laboratory, LBL-7098, p. 227-238.

Barker, C. E., 1979, Vitrinite reflectance geothermometry in the Cerro Prieto geothermal system, Baja California, Mexico (M.S. thesis): Riverside, University of California, 126 p.

de Boer, J., 1979, Paleomagnetic dating of the Cerro Prieto volcano (Abstract), in Program and Abstracts, Second Symposium on the Cerro Prieto Geothermal Field, Baja California, Mexico: Mexicali, Comisión Federal de Electricidad, p. 20-21.

Elders, W.A., 1979, The geological background of the geothermal fields of the Salton Trough, in Elders, W. A., ed., Guidebook: geology and geothermics of the Salton Trough (Field Trip No. 7, Geol. Soc. America Annual Meeting, San Diego): University of California Riverside Campus Museum Contributions No. 5, p. 1-19.

Elders, W.A., and Biehler, S., 1975, Gulf of California rift system and its implication for the tectonics of western North America: Geology, v. 3, no. 2, p. 85

Elders, W. A., et al., 1972, Crustal spreading in southern California: Science, v. 178, p. 15-24.

_____, 1978, A comprehensive study of samples from geothermal reservoirs: Petrology and light stable isotope geochemistry of twenty-three wells in the Cerro Prieto geothermal field, Baja California, Mexico: Riverside, University of California, Institute of Geophysics and Planetary Physics, Rept. UCR/IGPP-78/26, 264 p.

_____, 1979 Hydrothermal mineral zones in the geothermal reservoir of Cerro Prieto, in Proceedings, First Symposium on the Cerro Prieto Geothermal Field, Baja California, Mexico, September 20-22, 1978: Berkeley, Lawrence Berkeley Laboratory, LBL-7098, p. 68-75.

Fonseca L., H., and Razo M., A., 1979, Gravimetric, magnetometric and seismic reflection studies at the Cerro Prieto geothermal field (Abstract), in Program and Abstracts, Second Symposium on the Cerro Prieto Geothermal Field, Baja California, Mexico: Mexicali, Comisión Federal de Electricidad, p. 36-37.

Foster, N. H., 1979, Geomorphic exploration used in the discovery of Trap Spring field, Nye County, Nevada, in Newman, G. W., and Goode, H. D., eds., Basin and Range Symposium: Rocky Mountain Assoc. Geol. and Utah Geol. Assoc., p. 477-486.

Howard, J. H., et al., 1978, Geothermal resource and reservoir investigations of U.S. Bureau of Reclamation leaseholds at East Mesa, Imperial Valley, California: Berkeley, Lawrence Berkeley Laboratory, LBL-7094, 305 p.

Hunt, C. B., 1969, Geologic history of the Colorado River, in Rabbitt, M. C., et al., The Colorado River region and John Wesley Powell: USGS Prof. Paper 669, p. 59-130.

Lyons, D. J., 1978, Sandstone reservoirs: Petrography, porosity-permeability relationship and burial diagenesis: Japan National Oil Corporation, Technical Research Center Report, no. 8, p. 1-69.

____, 1979, Organic metamorphism and sandstone porosity prediction from acoustic data: Japan National Oil Corporation, Technical Research Center Report, no. 9, p. 1-51.

Majer, E. L., et al., 1979, Seismological studies at Cerro Prieto, in Proceedings, First Symposium on the Cerro Prieto Geothermal Field, Baja California, Mexico, September 20-22, 1978: Berkeley, Lawrence Berkeley Laboratory, LBL-7098, p. 239-245.

Mañon M., A., et al., 1977, Extensive geochemical studies in the geothermal field of Cerro Prieto, Mexico: Berkeley, Lawrence Berkeley Laboratory, LBL-7019, 113 p.

Prian C., R., 1979a, Lithologic correlations of the Cerro Prieto wells based on well log interpretation, in Proceedings, First Symposium on the Cerro Prieto Geothermal Field, Baja California, Mexico, September 20-22, 1978: Berkeley, Lawrence Berkeley Laboratory, LBL-7098, p. 49-56.

_____, 1979b, Development possibilities at the Cerro Prieto geothermal field (Abstract), in Program and Abstracts, Second Symposium on the Cerro Prieto Geothermal Field, Baja California, Mexico: Mexicali, Comisión Federal de Electricidad, p. 49-56.

Puente C., I., and de la Peña L., A., 1979, Geology of the Cerro Prieto geothermal field, in Proceedings, First Symposium on the Cerro Prieto Geothermal Field, Baja California, Mexico, September 20-22, 1978: Berkeley, Lawrence Berkeley Laboratory, LBL-7098, p. 17-40.

Razo M., A., and Fonseca L., H., 1978, Prospección gravimetrica y magnetometrica en el valle de Mexicali, B.C.: Mexicali, Comisión Federal de Electricidad Rept., 34 p.

Razo M., A., Arellano G., F., and Fonseca L., H., 1978 CFE resistivity studies at Cerro Prieto, in Proceedings First Symposium on the Cerro Prieto Geothermal Field, Baja California, Mexico, September 20-22, 1978: Berkeley, Lawrence Berkeley Laboratory, LBL-7098, p. 167-178.

Smith, J. L., 1979, Geology and commercial development of the East Mesa Geothermal Field, Imperial Valley, California, in Elders, W. A., ed., Guidebook: Geology and geothermics of the Salton Trough (Field Trip No. 7, Geol. Soc. America Annual Meeting, San Diego): University California, Riverside Campus Museum Contributions No. 5, p. 86-94.

Stephen, M. F., and Gorsline, D. S., 1975, Sedimentary aspects of the New River delta, Salton Sea, Imperial County, California, in Broussard, M. L., ed., Deltas -- models for exploration: Houston Geological Society, p. 267-282.

Truesdell, A. H., et al., 1979, Geochemical studies of the Cerro Prieto reservoir fluid (Abstract) in Program and Abstracts, Second Symposium on the Cerro Prieto Geothermal Field, Baja California, Mexico: Mexicali, Comisión Federal de Electricidad, p. 28-31.

van de Kamp, P. C., 1973, Holocene continental sedimentation in the Salton Basin, California: A reconnaissance: Geol. Soc. America Bull., v. 84, p. 827-848.

____, 1976, Inorganic and organic metamorphism in siliciclastic rocks (Abstract): AAPG Bulletin, v. 60, no. 4, p. 729.

Wagoner, J. L., 1977, Stratigraphy and sedimentation of the Pleistocene Brawley and Borrego formations in the San Felipe Hills area, Imperial Valley, California, U.S.A. (M.S. thesis): Riverside, University of California UCR/IGPP-77/24, 128 p.

Wilt, M. J., Goldstein, N. E., and Razo M., A., 1979, LBL resistivity studies at Cerro Prieto, in Proceedings, First Symposium on the Cerro Prieto Geothermal Field, Baja California, Mexico, September 20-22, 1978: Berkeley, Lawrence Berkeley Laboratory, LBL-7098, p. 179-188.

Woodard, G. D., 1974, Redefinition of Cenozoic stratigraphic column in Split Mountain Gorge, Imperial Valley, California: AAPG Bulletin, v. 58, p. 521-539.

TECHNICAL INFORMATION DEPARTMENT
LAWRENCE BERKELEY LABORATORY
UNIVERSITY OF CALIFORNIA
BERKELEY, CALIFORNIA 94720